Zircon U-Pb geochronology, Hf isotope, and petrochemical characteristics of Paleocene granitoids in western Gangdese Belt, Tibet

LIN JiQing[a,b,c], DING Feng[a,b,*], CHEN CuiHua[a,b], SHEN Tao[c]

[a] College of Earth Sciences, Chengdu University of Technology, Chengdu 610059, Sichuan, P. R. China

[b] Key Laboratory of Tectonic Controls on Mineralization and Hydrocarbon Accumulation of Ministry of Natural Resources, Chengdu University of Technology, Chengdu 610059, Sichuan, P. R. China

[c] 403 Geological Brigade of Sichuan Bureau of Geology and Mineral Resources, Emei 614200, P. R. China

* Corresponding author.

E-mail address: dfdingfeng@qq.com

Abstract: The research team studied the petrology, whole-rock geochemistry, zircon U-Pb age, and stable isotopic characteristics of the Nuocang area Rongguolongba and Garongcuo granites to better understand the impact of Neo-Tethys ocean subduction and India-Eurasia continental collision on Paleocene tectono-magmatic processes along the southern margin of the Gangdese Belt. Rongguolongba granite and Garongcuo granite porphyry were formed 61.86 Ma and 62.17 Ma, respectively. Nuocang granitoids are characterized by: 1) high SiO_2, NaO_2, and Al_2O_3 content-but low FeO^T, MgO, and TiO_2 content; 2) LREE and LILE enrichment-but HREE and HFSE (Nb, P, and Ti) depletion; 3) obvious negative Eu abnormalities. These features indicate that Nuocang granites are of the high-K cacl-alkaline and peraluminous granite types. Furthermore its zircon Hf isotope characteristics suggest that the magma source region has an ancient crystalline basement. The basaltic andesitic crystal tuff is the product of garnet-peridotite partial melting and crust contamination from rising magma emplacement.

Key words: Gangdese; Nuocang area; zircon U-Pb dating; Hf isotope

0. Introduction

The timing and process of the Indian-Eurasian continental collision is the most important scientific issue in Qinghai-Tibet Plateau research. Geologists are understandably concerned with this crucial event, as the plates' collision came to control the global tectonic framework, Asian landforms, surrounding ocean circulation, biogenetic derivation, and global climate change (Wang et al., 2003). The Gangdese Belt (Lhasa Block) is a massive magmatic tectonic belt located between the Yarlung Zangbo Suture Zone (YZSZ) and the Bangong-Nujiang Suture Zone (BNSZ), spanning about 2000 km east to west and 80 km north to south. Over 80% of the entire Qinghai-Tibet Plateau's magma distribution area is found in the Gangdese Belt. These magmatic rocks record rich information about tectonic evolution and deep Gangdese Belt processes, serving as a "probe" and "window" to the Tethys Ocean subduction and continental collision dynamics (Chung et al., 2003; Dong et al., 2005; Mo et al., 2005, 2009; Pan et al., 2006; Hou et al., 2008; Ji et al., 2009a, b; Xu et al., 2010; Zhu et al., 2011, 2015, 2017; Zhang et al., 2013, 2017; Tang et al., 2015; Wang et al., 2015a; Sun et al., 2017). Researchers have ascertained—based on the paleomagnetics, paleontology, tectonics, sedimentary petrology, magmatic petrology, and metamorphic

petrology—that the timeframe for initial collision between the Indian and Eurasian continents is limited to 70-34 Ma (Garzantie et al., 1987; Searle., 1987; Dewey., 1989; Rowley., 1998; Yin and Harrison., 2000; Aitchison., 2006). Hou et al. (2006) further restrict this window to 65 Ma according to regional petrology, isotopic chronology, and paleogeographic evidence. Thus, Paleocene-Eocene granite is highly significant to our understanding of this continental collision process. Collision-related volcanic rocks, intrusions, and dykes are distributed largely across the Gangdese Belt. Intrusive rocks are comprised of a series of small granite batholiths and intermediate-basic dykes. However, its volcanic rocks are of the Late Cretaceous-Eocene Linzizong Group, which can be further divided into the Dianzhong Formation, Nianbo Formation, and Pana Formation (from bottom to = top). volcanic strata are widely distributed across the southern Gangdese Belt. The diagenetic ages of the Dianzhong Formation, Nianbo Formation, and Pana Formation range from 68.7 to 59 Ma, 56 to 52 Ma, and 52 to 48 Ma, respectively (Jiang et al., 2018). The Linzizong Group in the eastern and western Gangdese belt has a similar diagenetic age, but diverge in terms of rock type and composition. The Nianbo Formation and Pana Formation are relatively developed in the western Gandese Belt. (Yu et al., 2010; Xie et al., 2013; Fu et al., 2014., Bao et al., 2014; Dong et al., 2017; Jiang., 2018). Linzizong volcanic rocks are the product of India and Eurasia's collision. A regional unconformity corresponding to the proposed collision date of 65 Ma exists between the Linzizong Group volcanic rocks and lower strata, thus possibly marking the continental collision event.. Linzizong Group volcanic rocks may therefore represent the thickening of the southern Lhasa Block continental crust during the subduction of the Tethys Oceanic Crust and transition to collision (Wang et al., 2007; Mo et al., 2008, 2009; Mo and Pan., 2006; Lu et al., 2015; Dong et al., 2017).

Theoretical research on Gangdese Belt Linzizong volcanic rocks has intensified in recent years, and interest in contemporaneous intrusions has grown. For example, granite porphyry at the western margin of the Linzhou Basin with a SHRIMP age of 58.7 Ma has been interpreted as the result of partial melting caused by crustal shortening and heating during early-stage collision between India and Eurasia starting about 65 Ma (Wang et al., 2006). Meanwhile, a study by Liu et al. (2016) finds, by petrogeochemical and isotopic dating, that the zircon U-Pb age of granites in the t eastern Gangdese batholith are 57.6-68.7 Ma, indicating the same provenance with different proportions of crust to mantle (Liu et al., 2016). Wang et al. (2018) believe that Riduo granite and

granodiorite dykes with zircon U-Pb ages of 59.5-62.7 Ma formed by the partial melting of basic lower crustal materials in the background of continuous northward subduction of the New Tethyan Ocean. The above referenced studies focus mainly on the eastern Gangdese Belt, while there has been little research conducted on western Gangdese Belt Paleocene granite. Nuocang area granitic bodies of the western Gangdese Belt are mainly granite and granite porphyry. In this paper, we present this granite's Zircon U-Pb chronology, whole rock geochemical, and zircon Hf isotope analysis. In combination with regional geological data, we aim to explain characteristics of the India-Eurasia collision along with the age, provenance, and genesis of the Gangdese Belt granitoids .

1. GEOLOGICAL BACKGROUND

The Qinghai-Tibet Plateau is separated by the Jinshajiang Suture Zone (JSSZ), Bangonghu-Nujiang Suture Zone (BNSZ), and Yarlungzangbo Suture Zone (YZSZ) with an E-W trend into the Songpan-Ganzi Terrane, Qiangtang Terrane, Lhasa Terrane, and Himalaya Terrane from north to south (Li et al., 1987; Yin and Harrison., 2000; Pan et al., 2006; Xu et al., 2011; Zhang et al., 2017; Liu et al., 2018, 2019) (Fig 1b). By its basement properties, the Lhasa Terrane (Gangdese Belt) can also be separated from north to south by the Shiquanhe-Namu Tso ophiolite mélange Fault (SNMF) and the Luobadui-Milashan Fault (LMF) into the North Lhasa Terrane (NL), Central Lhasa Terrane (CL), and South Lhasa Terrane (SL) (Zhu et al., 2009, 2011, 2013).

In the North Lhasa Terrane (NL), large-scale Jurassic-Cretaceous magmatic rocks developed, possibly with the southward subduction of the Bangonghu-Nujiang Ocean lithosphere and slab break-off following collision with the Qiangtang Terrane (Mo et al., 2005; Pan et al., 2006; Zhu et al., 2006; Zhang et al., 2010, 2012; Zhang et al., 2011; Zhu et al., 2013; Yan et al., 2017). Precambrian basement of the Central Lhasa Terrane (CL) crystalline basement is currently identified as the Neoproterozoic Nianqingtanggula Group as found on the west bank of Namu Tso (Hu et al., 2005; Zhang et al., 2010; Dong et al., 2011). Its sedimentary cover is Ordovician-Cenozoic volcanic sedimentary sequence with Permian-Eocene magmatic developments related to the opening, subduction, and closure of the Tethys ocean in conjunction with different terranes,

break-up and collision between different terranes (Pan et al., 2006; Zhu et al., 2011, 2013). The South Lhasa Terrane (SL) is characterized by large-scale distribution of Meso-Cenozoic magmatic rocks-including the famous Gangdese batholith and Linzizong volcanic rocks-as well as minor Triassic–Cretaceous volcanic-sedimentary rocks (Zhu et al., 2011, 2013; Zhang et al., 2013). At present, Hf isotope mapping shows the Lhasa Terrane's NL and SL are dominated by juvenile crustal materials, while its CL is characterized by ancient crust (Zhang et al., 2013; Zhu et al., 2013; Zhang et al., 2018).

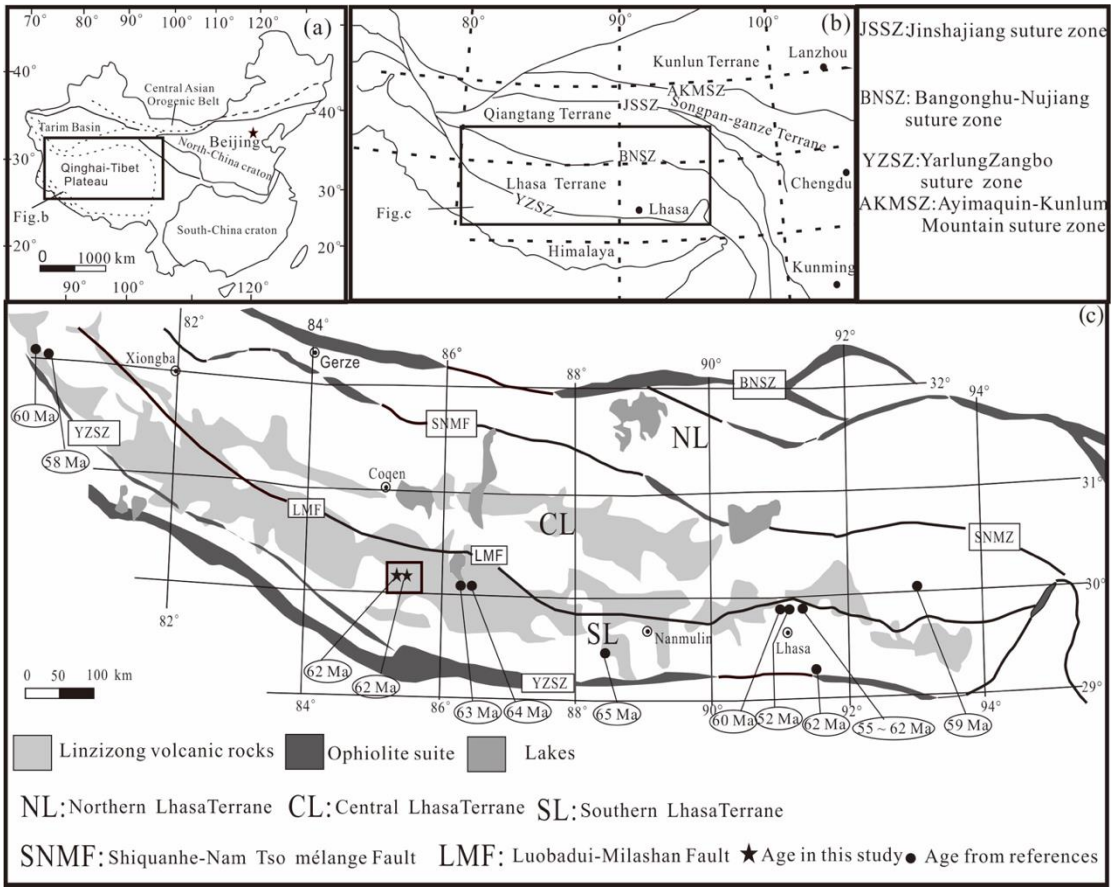

Fig. 1. a. Tectonic sketch map of China (after Zhang et al., 2014). b. Tectonic sketch map of Qinghai-Tibet Plateau. c. Simplified tectonic units of Lhasa Terrane (after Zhu et al., 2013). References age data sources are the same as in Table 4

The study area is located in the southern margin of the Gangdese Belt's Coqen Basin adjacent to the junction of the Central (CL) and South Lhasa Terranes (SL) (Fig. 1c). Here, mainly developed the sedimentary strata include (1) the Late Cretaceous-Eocene Linzizong volcanic succession and the Carboniferous-Permian metasedimentary series (Yongzhu Formation, Laga Formation and the Angjie Formation). The Linzizong volcanic rocks create an unconformity with

the Carboniferous-Permian metasedimentary series below. Linzizong volcanic rocks only developed the Dianzhong Formation and Nianbo Formation in this area, which are of the calc-alkaline series. The Dianzhong Formation is composed of clastic crystalline tuff and a small amount of basalt. The Nianbo Formation is composed of gray-green rhyolitic tuff, rhyolite and dacite, volcanic breccia, sandstone and conglomerate (Bao et al., 2013; Ding et al., 2017) (Fig. 2).

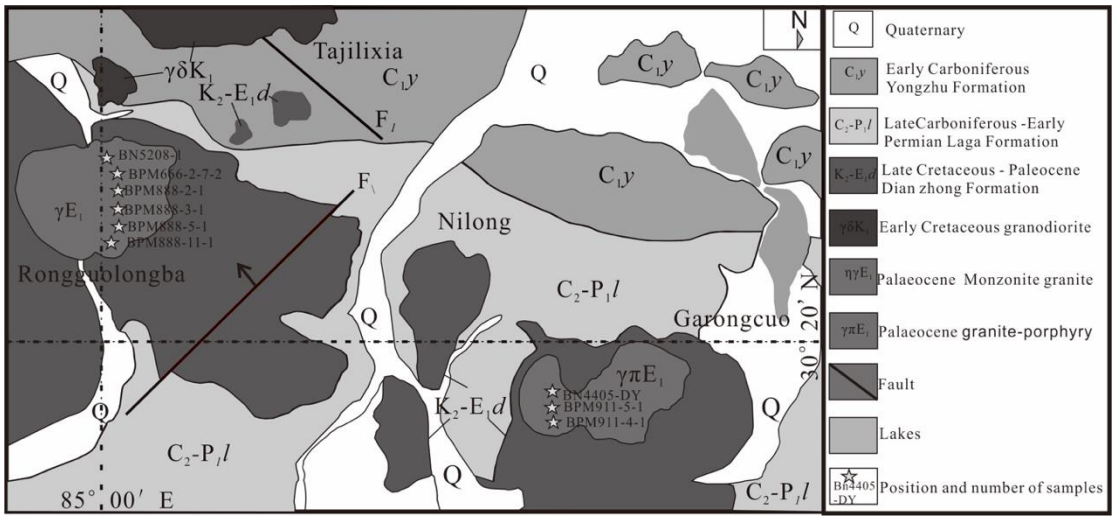

Fig 2. Geological map of study area.

2. GEOLOGY OF THE NUOCANG GRANITOID

Paleocene Rongguolongba granite composition is 50% plagioclase, 20-30% quartz, and 10-15% orthoclase, chlorite, and biotite. Accessory minerals include opaque minerals such as apatite and zircon. Some granite shows sericitization, clayization, and chloritization (Fig. 3b).

Garongcuo granite porphyry has a porphyritic texture (Fig. 3c). Phenocrysts account for about 35% of volume, of which biotite, plagioclase, potassium feldspar, and quartz account for 5%, 10%, 15%, and 5%, respectively. Plagioclase, potassium feldspar, and quartz particle sizes range from 0.3 to 1.0 mm, 0.2 to 2.3 mm, and 0.3 to 2 mm, respectively. The Garongcuo granite porphyry is 65% matrix, which is composed of plagioclase, potassium feldspar, and quartz, with particle sizes under 0.1 mm.

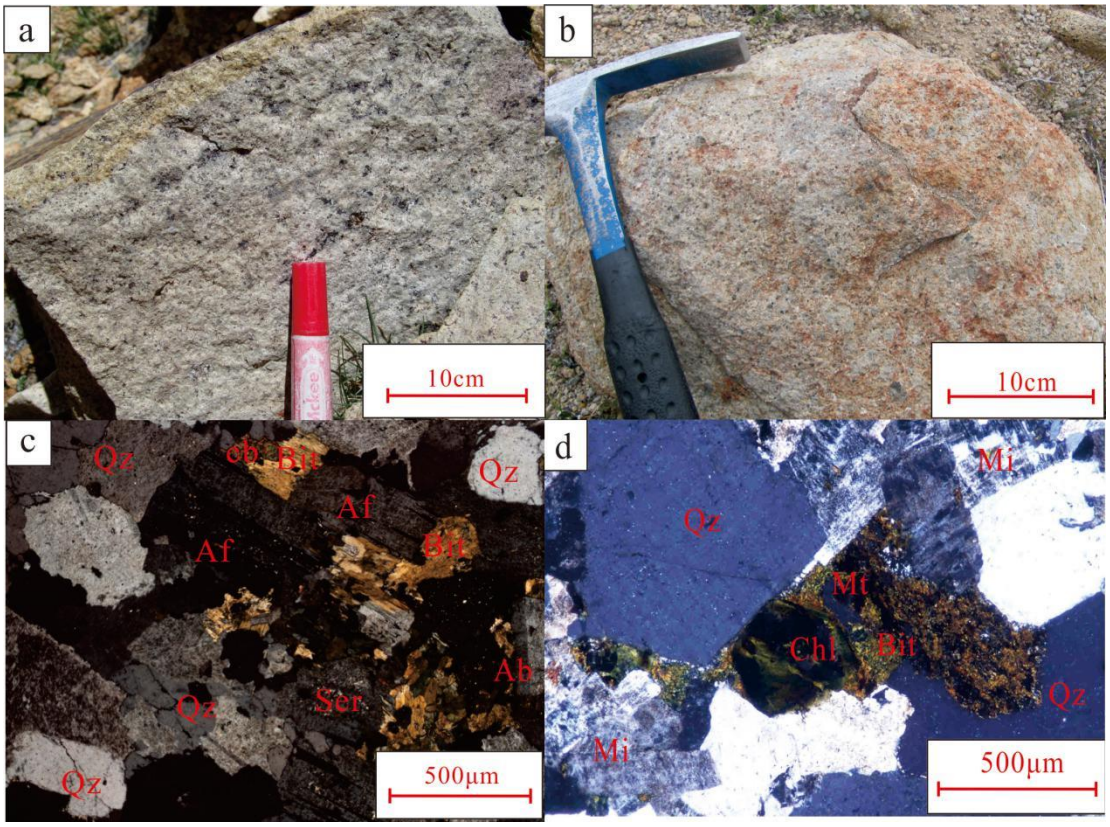

Fig. 3. The outcrops of Guoluolongba granite in Nuocang area,Tibet (a); The outcrops of Garongcuo granite porphyry in Nuocang area,Tibet (b); Photomicrograph of granite (c); Photomicrograph of granite.（d）

Qz = quartz, Pl = plagioclase, Or = orthoclase feldspar, Bit = biotite, Mi = microcline feldspar，Ser = sercite，Pl = plagioclase, Ab = albite, and Cc = clacite.

3. Methodology

Samples in this study were bedrock with weak surface weathering. Weathered surface layers were removed from samples before analysis. The agate mortar was cleaned with chemical ethanol in advance to prevent sample contamination. Zircon target and cathodoluminescence microphotography (CL) were conducted in the laboratories of Beijing Zhongke Mine Research and Testing Technology Co., Ltd. The specific preparation process is detailed by Song et al. (2015). Zircon U-Pb isotope dating was conducted with the Agilent 7500a ICP-MS at the State Key Laboratory of Geochemistry of Deposits, Institute of Geochemistry, Chinese Academy of Sciences. Laser beam diameter was 30 um. Standard zircon 91500 (1064 Ma) (Wiedenbeck et al., 1995) and GJ-1 (600 Ma) served as external standards and NISTSRM610 ^{29}Si as the internal standard. The error standard in the test was 1σ. The analysis data were processed by ICP-MSDataCal 9.2.

A Zircon Hf isotope test was conducted with Neptune plus multi-receiver plasma mass spectrometry (MC-ICP-MS) and an NWR213nm solid-state laser in the Beijing Zhongke Mine Research and Testing Technology Co., Ltd laboratory. During the experiment, helium was used to carry the denudation material, and the denudation diameter was 55 um. Zircon GJ-1 and Plesovice served as reference materials. The analysis point was in the same position as the U-Pb dating analysis point. The detailed analytical procedures and operating conditions were similar to those described by Hou et al. (2007). The weighted average values of $^{176}Hf/^{177}Hf$ of zircon standard GJ-1 were 0.282007±0.000007 (2σ, n = 36), completely consistent with those reported in Hou et al. (2007) and Morel et al. (2008).

Samples were ground to 200 mesh and sent to Southwest Metallurgical Geological Testing Institute of Sichuan Province for chemical analysis. Major elemental analysis was determined by PHILLIPSPW-2404 X-ray fluorescence spectrometer with accuracy better than 1%. Trace and rare earth elemental analysis was determined by ELEMENT-2 mass spectrometer with accuracy better than 2%. The detailed analysis process can be found in Fei et al. (2014).

4. Geochemical and isotopic composition

Table 1 shows representative major, trace, and rare-earth element compositions of rock samples from the Nuocang area of Tibet.

Major and trace elements. Major and trace elements from 11 granitoid samples, taken from two Paleocene intrusions (RongguoLongba and Garongcuo), as well as five basaltic andesitic crystal tuff samples from the Dianzhong Formation in Nuocang (data from Jiang et al., 2018) are listed in Table 1 (BPM911-6-1, BPM911-12-1 from Wang et al., 2017). The major element characteristics of the two granite rock samples are not significantly different. SiO_2 content ranges from 70.47wt.% to 77.11wt.%; Al_2O_3, K_2O, P_2O_5, TiO_2, MgO content ranges from 12.34wt.%, 13.41wt.%, 3.02wt.%,. 5.38wt%, 0.01wt.%, 0.06wt.%, 0.09wt.%, 0.24wt.%, 0.06wt.% and 0.24wt.%, respectively; samples' K_2O/Na_2O varies between 0.89 and 2.0; Rittmann Index ranges from 1.67 to 1.99, indicating a calc-alkaline rock affinity [$\delta=(Na_2O+K_2O)^2/(SiO_2-43)$]. DI Index ranges from 82.82 to 94.05, indicating the rock is highly fractionated. The analyzed samples have high Na_2O+K_2O content, between 6.91wt.% and 8.23wt.%. On the SiO_2 vs. Na_2O+K_2O (TAS)

diagram (Fig. 6a), all samples plot in the granite field, and with A/CNK (molar $Al_2O_3/CaO+K_2O$) ratios varying between 0.88 and 1.16.on the SiO_2-KO_2 diagram, all fall into the high-K calc-alkaline series classification (Fig.7d). Based on this study's dating results, there is no clear rule governing changes in the production of the above major elements. Granitoid and eastern Gangdese intrusive rock samples are compositionally analogous to the volcanic rocks of the Dianzhong Formation in Nuocang area(Fig.4a).

Dianzhong Formation basaltic andesitic crystal tuff is characterized by low SiO_2 and K_2O content ranging from 53.93-55.84 wt.% and 1.33-1.63 wt.%, respectively, as well as low A/CNK 0.85-0.95, high Na_2O, MgO, TiO_2, and TFeO-content ranging from 2.68-3.3 wt.%, 3.76-4.9 wt.%, 1.13-1.19 wt.%, and 6.1-8.1, respectively. On the SiO_2 vs.Na_2O+K_2O (TAS) diagram (Fig. 4c), all samples plot onto the basalt-andesite field. $Mg^{\#}$ value ranges from 47 to 52, indicating the basic volcanics.

RongguoLongba granite and Garongguo granite porphyry generally have similar REE patterns displaying LREE-enrichment and obvious fractionated HREE relative to LREE—LREE/HREE = 5.82-13.98, La_N/Yb_N = 4.6-17.84, δEu = 0.21-0.61-with a negative Eu anomaly (Fig. 5a). In the primitive mantle-normalized spider diagram (Fig.5b), all granite and granite porphyry samples are characterized by enrichments of incompatible elements and LILE—such as Rb, Ba, Th, K-and pronounced depletions of high field elements (HFSE), such as Nb, Sr, Ti, and P. In terms of trace element composition, the samples in this study are similar to magmatic rocks of the eastern Gangdese Belt in Tibet. The basic volcanics rare earth partition curve is smooth. The samples exhibit weak negative Eu anomalies (Eu/Eu* = 0.87–0.91) and fractionated REE patterns characterized by $(La/Yb)_N$ ratios of 9.98–10.79 (Table. 1). As shown in the primitive mantle-normalized spider diagram, these samples are characterized by enrichments of incompatible elements and LILE such as Rb and K, and high field element (HFSE) depletions such as Nb and U (Figure 5b). Sr and Y content is high, ranging from 685-713.8 ppm and 18.8-20.8 ppm, respectively.

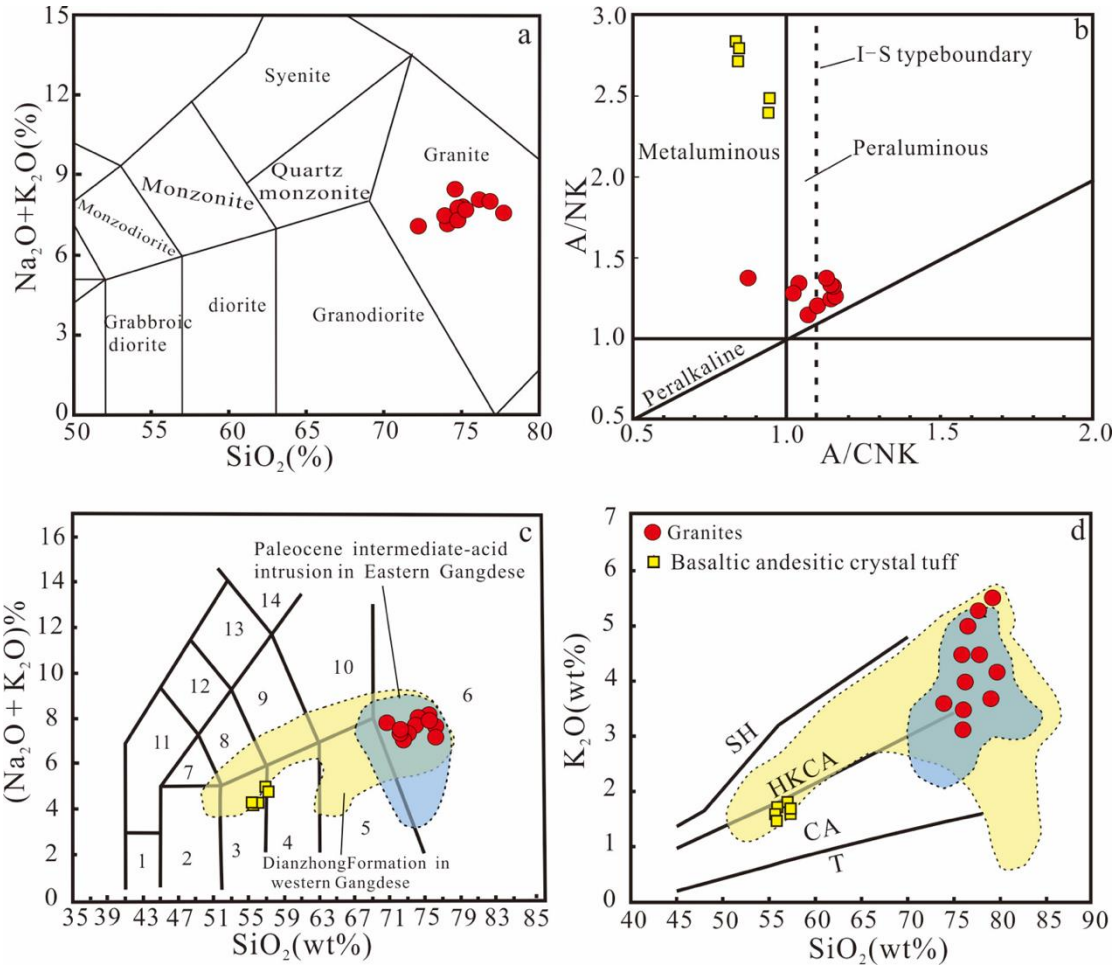

Fig. 4 Total alkali vs. silica (a) (Wilson, 2001)； A/NK vs A/CNK (b)； total alkali vs. silica (TAS) (c) Total alkali vs. silica (Le Maite, 2002)； K_2O-SiO_2 plot (d) (Rickwood, 1989). Nuocong area Linzizong Dianzhong Formation data are as in Hu (2011), Bao (2013), and Jiang (2018); Eastern Gangdese Belt intrusion data are as in Wang et al. (2006), Dong et al. (2015), Li et al. (2012), and Wang et al. (2019).

1 = picrite-basalt; 2 = basalt; 3 = basalt-andesite; 4 = andesite; 5 = dacite; 6 = rhyolite; 7 = trachybasalt; 8 = basaltic trachy-andesite; 9 = amygdaloidal andesite; 10 = trachyte; 11 = tephrite; 12 = phonolitic tephrite; 13 = tephritic phonolite; 14 = phonolite.

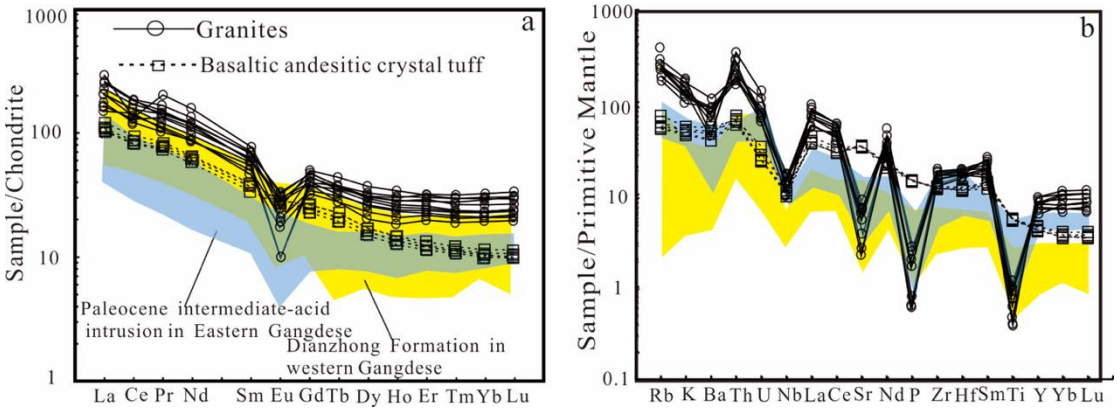

Fig. 5 Chondrite-normalized REE patterns (a, *normalization values from* Sun and McDonough,1989) and primitive mantle-normalized trace element patterns (b) for Nuocang intermediate-acid dykes = (*normalization values from* Pearce et al., 1984).

Lu-Hf isotopic characteristics. The research team conducted Lu-Hf isotope analysis with zircon age on the granite porphyry (BN4405-DY) and granite (BN5208-1). Results are given in Table 2 and positions shown in Fig 6. The zircon $^{176}Hf/^{177}Hf$ ratio of the granite porphyry (BN4405-DY) is 0.282520-0.282641; the $\varepsilon_{Hf}(t)$ value is -7.38--4.12; the mantle model age is 870-1047 Ma, and the crustal model age (T_{DM}^{C}) is 1356-1615 Ma. The zircon $^{176}Hf/^{177}Hf$ ratio of granite (BN5208-1) is 0.282529-0.282621; the $\varepsilon_{Hf}(t)$ value is 7.48-3.61; the mantle model age is 928-1042 Ma, and the crustal model age (t_{DM}^{C}) is 1394-1601 Ma.

Table 1. Major (wt.%) and trace (ppm) element contents of representative granite and granite porphyry samples

Sample	BN5208-1	BPM666-2-7-2	BPM888-2-1	BPM888-3-1	BPM888-5-1	BPM888-11-1	BPM911-4-1	BPM911-5-1	BN4405-DY	BPM911-6-1	BPM911-12-1
Component	1	2	3	4	5	6	7	8	9	10	11
SiO_2	74.87	73.58	75.81	77.11	73.5	73.71	70.47	72.63	76.08	72.97	73.28
TiO_2	0.14	0.19	0.1	0.09	0.18	0.18	0.24	0.23	0.13	0.23	0.19
Al_2O_3	12.81	13.13	12.36	12.42	13.01	13.04	12.96	13.25	12.34	13.41	13.07
Fe_2O_3	0.42	0.33	0.76	0.52	0.98	0.77	1.78	1.29	0.58	1.27	1.78
FeO	1.74	1.79	1.17	0.99	1.91	1.55	1.68	2.19	1.47	2.03	0.89
MnO	0.03	0.07	0.02	0.04	0.04	0.04	0.05	0.06	0.03	0.04	0.04
MgO	0.17	0.22	0.06	0.06	0.17	0.17	0.23	0.24	0.1	0.19	0.09
CaO	0.47	0.88	0.34	0.42	1.54	1.4	2.96	0.85	0.28	1.02	0.62
Na_2O	2.76	3.08	2.64	3.42	3.36	3.31	3.48	3.8	4.15	4.06	3.3
K_2O	5.21	4.38	5.38	4.14	3.93	4.39	3.43	3.47	3.67	3.02	4.93
P_2O_5	0.03	0.04	0.01	0.01	0.04	0.04	0.06	0.06	0.02	0.06	0.04
LOI	1.35	2.31	1.36	0.78	1.35	1.41	2.68	1.93	1.15	1.69	1.83
Total	100.00	100.00	100.01	100.00	100.01	100.01	100.02	100.00	100.00	99.99	100.06
Rb	251.2	154.9	187.3	154.6	157.6	164.3	125.3	125.1	145.55	118.2	159.7
Sr	107.3	129.9	53.86	50	128.4	113.8	183.2	137.1	80.17	155.1	152
Y	14.3	33.75	43.79	43.86	37.79	38.9	35.56	36.31	36.91	32.86	28.04
Zr	104.78	176.72	145.1	141.67	172.16	183.29	199.46	186.22	183.35	217.46	168.06
Nb	6.83	9.15	9.33	7.71	10.08	9.94	12.26	7.54	10.09	11.4	7.28
Ba	547.9	540.3	314.3	311.45	530.3	429.1	587.2	636.1	643.25	658.4	794.2
La	37.9	49.68	48.53	35.36	48.03	38.68	52.48	59.55	41.46	59.21	58.4
Ce	71.76	82.1	96.05	86.92	94.48	78.57	101.72	108.35	74.19	110.27	108.39
Pr	7.77	10.56	11.39	10.16	13.31	12.55	13.48	15.42	9.42	12.71	13.93
Nd	30.14	41.31	44.59	39.37	54.2	48.86	54.41	59.77	40.11	51.2	52.74
Sm	4.46	7.11	8.82	8.45	10.61	9.57	10.19	10.64	7.53	9.08	8.95
Eu	0.73	0.99	0.59	0.57	1.42	1.12	1.92	1.8	1.18	1.72	1.62
Gd	3.84	6.64	8.27	7.72	10.21	9	9.41	9.52	7.14	8.23	9.03
Tb	0.51	1.03	1.4	1.32	1.63	1.35	1.39	1.37	1.15	1.18	1.28

Dy	2.55	5.88	8.27	7.86	9.33	7.66	7.66	7.48	6.61	6.49	7.1
Ho	0.5	1.18	1.76	1.71	1.92	1.59	1.6	1.48	1.35	1.32	1.42
Er	1.54	3.55	5.11	5.27	5.17	4.79	4.61	4.21	3.95	3.73	4.08
Tm	0.22	0.52	0.75	0.81	0.75	0.67	0.7	0.6	0.59	0.54	0.59
Yb	1.52	3.54	5.14	5.51	5.02	4.47	4.87	3.93	3.87	3.56	3.95
Lu	0.25	0.53	0.78	0.85	0.75	0.68	0.78	0.61	0.6	0.55	0.62
Hf	3.61	5.52	4.83	4.75	5.19	5.67	5.84	5.54	5.55	6.13	5.2
Th	24.5	19.08	28.79	25.62	16.42	21.08	15.66	15.02	17.06	16.6	17.02
U	1.73	1.59	2.85	1.39	1.37	1.79	1.59	1.98	1.46	1.79	2.32
ΣREE	163.68	214.65	241.46	211.89	256.83	219.56	265.19	284.74	199.12	269.81	272.11
LREE	152.75	191.77	209.98	180.83	222.05	189.35	234.19	255.53	173.88	244.2	244.02
HREE	10.93	22.89	31.48	31.05	34.78	30.21	31	29.21	25.24	25.62	28.08
LREE/HREE	13.98	8.38	6.67	5.82	6.38	6.27	7.55	8.75	6.89	9.53	8.69
La_N/Yb_N	17.84	10.06	6.77	4.6	6.87	6.2	7.73	10.87	7.69	11.92	10.6
δEu	0.54	0.44	0.21	0.21	0.42	0.37	0.6	0.55	0.49	0.61	0.55
δCe	1.03	0.88	1	1.12	0.92	0.87	0.94	0.88	0.92	0.99	0.93
$Mg^{\#}$	9.37	11.93	4	5.01	7.27	8.89	8.28	8.44	6.07	7.14	4.53
σ	1.99	1.8	1.95	1.67	1.73	1.92	1.71	1.77	1.84	1.66	2.22
Q	36.85	36.26	38.97	40.1	34.72	34	31.8	34.56	36.56	34.9	34.1
An	2.33	4.33	1.7	2.09	7.64	6.93	9.9	4.07	1.46	4.93	3.09
Ab	23.7	26.68	22.6	29.13	28.83	28.41	30.22	32.81	35.53	34.9	28.43
C	1.8	1.81	1.61	1.57	0.47	0.35	0	1.81	1.02	1.72	1.22
Hy	3.15	3.47	1.56	1.47	2.93	2.46	0	3.34	2.34	2.9	0.92
Ilm	0.27	0.36	0.19	0.17	0.34	0.34	0.46	0.45	0.26	0.45	0.36
Mt	0.61	0.49	1.12	0.76	1.44	1.13	2.64	1.91	0.84	1.87	2.13
Ap	0.06	0.1	0.03	0.03	0.09	0.08	0.13	0.14	0.04	0.14	0.09
Zr	0.02	0.04	0.03	0.03	0.03	0.04	0.04	0.04	0.04	0.04	0.03
DI	91.78	89.43	93.78	93.89	87.08	88.7	82.82	88.28	94.05	87.97	92.18
A/CNK	1.16	1.15	1.15	1.14	1.03	1.02	0.88	1.15	1.09	1.14	1.1

Table 1 (*continued*)

Sample	NCH-HSY3-1	NCH-HSY6	NCH-HSY7	NCH-HSY4	NCH-HSY5
Component	12	13	14	15	16
SiO_2	53.93	55.84	55.27	54.25	54.33
TiO_2	1.16	1.13	1.14	1.16	1.19
Al_2O_3	16.46	17.12	16.79	16.5	16.43
Fe_2O_3	2.59	2.75	2.98	2.36	2.27
FeO	5.75	5.2	5.25	5.85	5.9
MnO	0.13	0.13	0.13	0.13	0.14
MgO	4.9	3.76	4	4.73	4.66
CaO	7.8	6.49	6.34	7.99	7.86
Na_2O	2.68	3.23	3.19	2.68	2.7
K_2O	1.39	1.46	1.63	1.33	1.5
P_2O_3	0.31	0.3	0.3	0.31	0.31
LOI	2	1.75	2.12	1.79	1.76
Total	99.1	99.16	99.14	99.08	99.05
Rb	33.14	38.65	45.23	32.62	34.81
Sr	702.34	685.01	685.22	695.60	713.78
Y	20.13	20.78	18.21	18.87	18.79
Zr	128.67	138.18	133.67	129.75	130.83

Nb	6.84	8.68	7.90	7.38	7.96
Ba	269.06	319.05	374.12	270.08	338.59
La	26.11	29.18	25.00	24.48	24.69
Ce	53.57	58.34	50.06	50.72	51.03
Pr	7.76	8.10	7.03	7.44	7.36
Nd	30.01	30.61	26.51	28.69	28.73
Sm	6.03	6.01	5.16	5.72	5.69
Eu	1.69	1.63	1.49	1.58	1.56
Gd	5.39	5.48	4.68	5.17	4.98
Tb	0.84	0.85	0.72	0.78	0.78
Dy	4.28	4.32	3.79	4.04	4.09
Ho	0.81	0.83	0.71	0.76	0.75
Er	2.06	2.19	1.87	1.97	1.95
Tm	0.29	0.31	0.27	0.28	0.28
Yb	1.82	1.94	1.67	1.76	1.69
Lu	0.27	0.29	0.25	0.25	0.26
Hf	3.57	3.74	3.40	3.49	3.40
Th	4.86	6.06	5.54	5.44	5.22
U	0.50	0.56	0.69	0.48	0.49
ΣREE	140.92	150.07	129.22	133.65	133.84

LREE	125.17	133.87	115.25	118.63	119.06
HREE	15.76	16.21	13.96	15.01	14.78
LREE/HREE	7.94	8.26	8.26	7.90	8.06
La_N/Yb_N	10.29	10.79	10.74	9.98	10.48
δ Eu	0.91	0.87	0.93	0.89	0.90
δ Ce	0.92	0.93	0.93	0.92	0.93
Mg#	0.52	0.47	0.47	0.51	0.51
σ	1.4	1.62	1.77	1.33	1.45
Q	8.76	10.92	9.93	9.12	8.78
An	29.64	28.65	27.5	29.87	29.07
Ab	23.35	28.06	27.83	23.31	23.48
Hy	16.31	14.67	15.34	15.94	15.84
Mt	3.87	3.97	4.15	3.52	3.38
Ap	0.74	0.71	0.72	0.74	0.74
DI	40.58	47.84	47.69	40.51	41.37
A/CNK	0.85	0.95	0.94	0.84	0.84

Note.1-6, Rongguo Longba granite; 7-11, Garongcuo granite porphyry; 12-16, Nuocang area basaltic andesitic crystal tuff (*data from* Jiang., 2018); Q = quartz; An = anorthite; Ab = albite; Or = orthoclase; C = corundum; Hy = hypersthene; Ilm = ilmenite; Mt = magnetite; Ap = apatite; Zr = zircon; Chr = chromite. $Mg^{\#}$ = $100\times Mg^{2+}/(Mg^{2+}+Fe^{2+})$, in which Mg^{2+}, Fe^{2+} are molar fractions; (2) A/CNK = molar $Al_2O_3/(CaO+Na_2O+K_2O)$, (3) $\sigma = (Na_2O+K_2O)^2/(SiO_2-43)(wt\%)$, (4) DI = Qz+Or+Ab+Ne+Lc+Kp.

231

Table 2 . The zircon Hf isotopic compositions of Nuocang area granitic rock, southern Tibet

Spot number	Age(Ma)	Lu(ppm)	Hf(ppm)	$^{176}Yb/^{177}Hf$	$^{176}Lu/^{177}Hf$	2σ	$^{176}Hf/^{177}Hf$	2σ	$\varepsilon_{Hf}(0)$	$\varepsilon_{Hf}(t)$	t_{DM1}/Ma	t_{DM}^{c}/Ma	$f_{Lu/Hf}$
BN5208-1-01	62.1	80.6	12965	0.040752	0.001521	0.000012	0.282569	0.000023	-7.18	-5.95	980	1510	-0.95
BN5208-1-03	62.3	95.2	11963	0.048136	0.001651	0.000007	0.282621	0.000015	-5.34	-4.12	909	1394	-0.95
BN5208-1-05	61.8	80.5	12940	0.027172	0.001032	0.000005	0.282542	0.000019	-8.12	-6.88	1005	1570	-0.97
BN5208-1-06	63.1	72	13021	0.025714	0.000899	0.000001	0.282583	0.000014	-6.67	-5.41	944	1477	-0.97
BN5208-1-07	64.5	84.6	13098	0.025021	0.000918	0.000015	0.282595	0.000015	-6.25	-5	928	1451	-0.97
BN5208-1-09	61.3	73.8	12767	0.041254	0.001452	0.000009	0.28258	0.000017	-6.79	-5.52	962	1485	-0.96
BN5208-1-10	63.1	80.6	13351	0.045725	0.001701	0.000023	0.282529	0.000023	-8.59	-7.38	1042	1601	-0.95
BN5208-1-18	64.5	90.6	11636	0.038644	0.001425	0.000029	0.282555	0.000019	-7.69	-6.47	998	1543	-0.96
BN5208-1-19	61.7	69.3	15767	0.04584	0.001592	0.000033	0.28255	0.000015	-7.86	-6.63	1009	1553	-0.95
BN5208-1-20	62.0	71.2	13672	0.030678	0.001079	0.000024	0.282571	0.000016	-7.11	-5.84	966	1505	-0.97
BN5208-1-22	61.3	85	13232	0.031842	0.001053	0.000017	0.282594	0.000017	-6.3	-5.04	933	1454	-0.97
BN4405-Dy-01	61.1	95.9	8977	0.000182	0.00156	0.000007	0.282562	0.00002	-7.42	-6.25	991	1529	-0.95
BN4405-Dy-06	67.3	55.5	8778	0.000141	0.001308	0.000003	0.282604	0.000016	-5.94	-4.81	925	1435	-0.96
BN4405-Dy-07	59.9	70.1	9758	0.000157	0.001164	0.000007	0.282641	0.000021	-4.65	-3.61	870	1356	-0.96
BN4405-Dy-08	61.3	65	9739	0.001846	0.002081	0.000058	0.282551	0.000017	-7.8	-6.61	1021	1553	-0.94
BN4405-Dy-10	61.8	79.9	9064	0.000388	0.001197	0.000024	0.282616	0.000015	-5.53	-4.24	906	1404	-0.96
BN4405-Dy-11	62.3	100	9806	0.000286	0.00141	0.000013	0.28252	0.000022	-8.91	-7.48	1047	1615	-0.96
BN4405-Dy-12	61.5	89.7	8399	0.000193	0.001215	0.00001	0.282601	0.000018	-6.05	-4.35	927	1426	-0.96
BN4405-Dy-13	62.4	103.9	7555	0.000203	0.001128	0.000004	0.282587	0.000018	-6.55	-5.37	945	1473	-0.97
BN4405-Dy-15	59.9	119.3	7540	0.000172	0.000936	0.000005	0.282583	0.000017	-6.68	-5.37	945	1476	-0.97
BN4405-Dy-16	61.1	77.3	8844	0.00014	0.001168	0.000006	0.282545	0.000017	-8.03	-6.8	1005	1565	-0.96
BN4405-Dy-17	58.0	61.4	9414	0.000306	0.001409	0.000009	0.282578	0.000021	-6.85	-5.62	964	1490	-0.96

Isotope geochronology

One Nuocang granite sample (BN5208-1) and one granite porphyry sample (BN4405-DY) were selected for zircon U-Pb age analysis. Most of the zircons in the samples were transparent and subhedral, with lengths of 50–150 μm. Some grains exhibited concentric zoning, and some grains demonstrated core-mantle structure (Fig.6). The granite's Th and U content (BN5208-1) was 94.51×10^{-6}-443.54×10^{-6} and 266.89×10^{-6}–484.42×10^{-6}, respectively, and Th/U ratios were 0.28-1.12. The granite porphyry's Th and U content(BN4405-DY) measured 98.17×10^{-6}-342.75×10^{-6} and 90.77×10^{-6}-262.91×10^{-6}, respectively, while its Th/U ratios were 0.63-1.3. Th/U ratios were all greater than 0.1 (Table 3), and there was positive correlation between Th and U content. These characteristics indicate that the zircons evaluated in this study are magmatic zircons (Hoskin and Schaltegger, 2003; Wu and Zheng, 2004). The weighted mean zircon U-Pb age for the granite (BN5208-1) and granite porphyry samples (BN4405-Dy) are 61.86±0.8 Ma (MSWD = 0.60) and 62.17±0.67 Ma (MSWD = 0.052), respectively（Fig. 7).

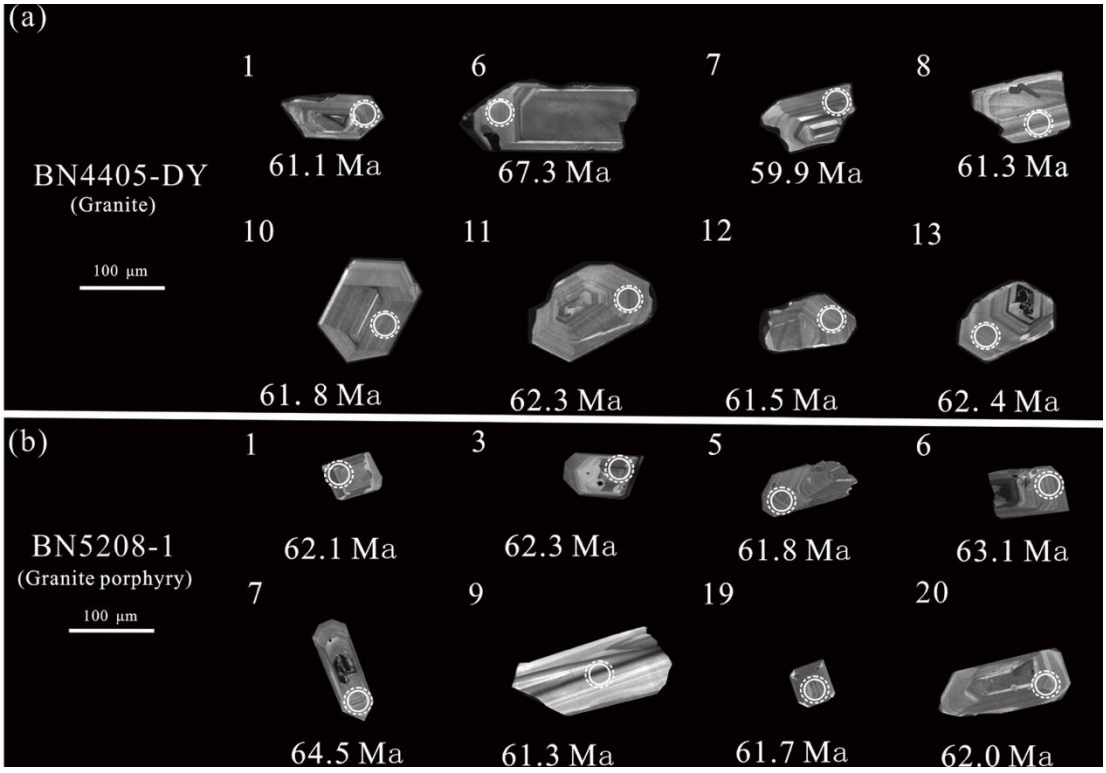

Fig. 6. Cathodoluminescence images of selected granite zircons(BN5208-1) (a) and granite porphyry zircons（BN4405-Dy）(b). Solid and dashed circles show the locations for U-Pb dating and Hf isotope dating, respectively.

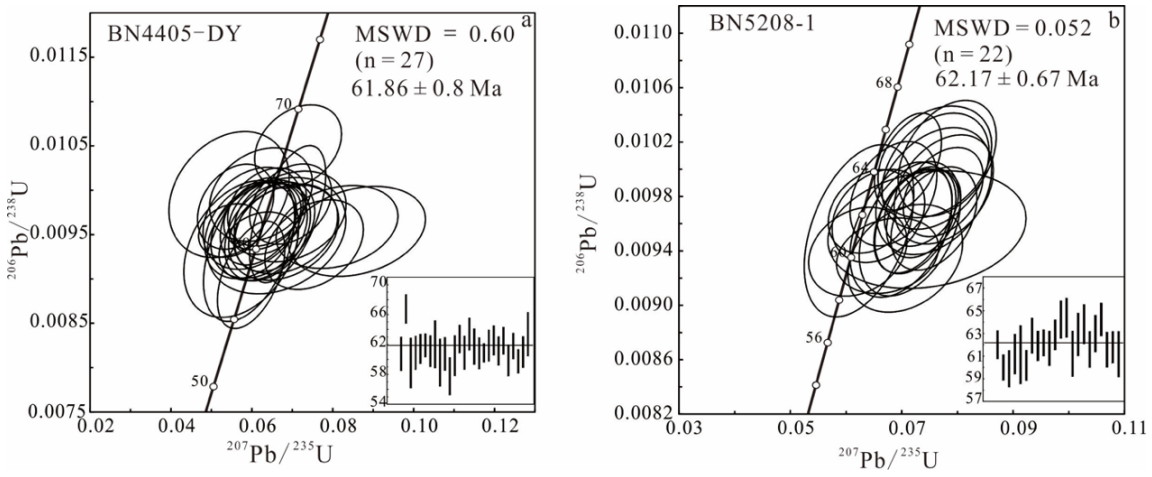

Fig. 7.ICP-MS zircon U-Pb dating concordia diagrams for granite samples (BN4405-DY and BN5208-1) from the Nuocang area, Tibet.

Table 3. LA-ICP-MS zircon U-Pb dating analytical data of granite samples

Spot	Pb	Th	U	Th/U	$^{207}Pb/^{206}Pb$	$^{207}Pb/^{206}Pb$	$^{207}Pb/^{235}U$	$^{207}Pb/^{235}U$	$^{206}Pb/^{238}U$	$^{206}Pb/^{238}U$	$^{208}Pb/^{232}Th$	$^{208}Pb/^{232}Th$	$^{207}Pb/^{235}U$	$^{207}Pb/^{235}U$	$^{206}Pb/^{238}U$	$^{206}Pb/^{238}U$	$^{208}Pb/^{232}Th$	$^{208}Pb/^{232}Th$
	($\times10^{-6}$)				Ratio	±1σ	Ratio	±1σ	Ratio	±1σ	Ratio	±1σ	Age (Ma)	±1σ	Age (Ma)	±1σ	Age (Ma)	±1σ
BN4405-DY	Granite porphyry，E:85°09′10"，N：30°24′03"																	
-1	2.29	146.62	206.61	0.71	0.0524	0.0061	0.0639	0.0070	0.0095	0.000361	0.002730	0.000185	62.9	6.7	61.1	2.3	55.1	3.7
-2	3.14	226.01	241.48	0.94	0.0497	0.0050	0.0714	0.0071	0.0105	0.000310	0.002991	0.000187	70.1	6.7	67.3	2.0	60.4	3.8
-6	1.54	101.51	143.83	0.71	0.0485	0.0078	0.0593	0.0074	0.0093	0.000534	0.002632	0.000294	58.5	7.1	59.9	3.4	53.1	5.9
-7	2.83	192.21	262.91	0.73	0.0451	0.0055	0.0596	0.0074	0.0095	0.000359	0.002389	0.000211	58.8	7.1	61.3	2.3	48.2	4.3
-8	2.58	159.75	236.15	0.68	0.0470	0.0047	0.0616	0.0062	0.0096	0.000313	0.002876	0.000179	60.7	6.0	61.8	2.0	58.1	3.6
-10	2.38	148.86	211.05	0.71	0.0481	0.0051	0.0626	0.0063	0.0097	0.000251	0.003035	0.000215	61.7	6.0	62.3	1.6	61.3	4.3
-11	3.21	228.58	276.53	0.83	0.0506	0.0057	0.0657	0.0065	0.0096	0.000333	0.003389	0.000269	64.6	6.2	61.5	2.1	68.4	5.4
-12	2.17	124.15	184.85	0.67	0.0484	0.0039	0.0689	0.0062	0.0097	0.000510	0.003991	0.000431	67.6	5.9	62.4	3.3	80.5	8.7
-13	1.71	129.81	158.90	0.82	0.0457	0.0068	0.0574	0.0094	0.0093	0.000509	0.002723	0.000388	56.7	9.0	59.9	3.3	55.0	7.8
-15	2.59	181.23	223.64	0.81	0.0526	0.0074	0.0679	0.0090	0.0095	0.000355	0.003057	0.000203	66.7	8.5	61.1	2.3	61.7	4.1
-16	1.98	116.91	188.46	0.62	0.0496	0.0056	0.0598	0.0055	0.0090	0.000399	0.002863	0.000244	59.0	5.3	58.0	2.5	57.8	4.9
-17	2.78	173.14	248.93	0.70	0.0504	0.0080	0.0661	0.0113	0.0095	0.000433	0.002892	0.000217	65.0	10.8	60.9	2.8	58.4	4.4
-18	5.47	154.47	179.82	0.86	0.0527	0.0057	0.0696	0.0067	0.0098	0.000299	0.002855	0.000320	68.3	6.3	63.1	1.9	57.6	6.4
-19	3.64	112.37	139.48	0.81	0.0481	0.0065	0.0618	0.0079	0.0096	0.000358	0.002874	0.000425	60.9	7.5	61.3	2.3	58.0	8.6
-20	3.48	101.85	134.86	0.76	0.0440	0.0057	0.0623	0.0084	0.0100	0.000348	0.002927	0.000325	61.3	8.0	63.8	2.2	59.1	6.6
-22	5.95	182.10	169.59	1.07	0.0475	0.0076	0.0603	0.0082	0.0097	0.000380	0.002662	0.000255	59.4	7.8	62.1	2.4	53.7	5.1
-24	3.60	108.86	163.25	0.67	0.0655	0.0075	0.0860	0.0112	0.0095	0.000335	0.002787	0.000359	83.8	10.4	61.2	2.1	56.3	7.2
-25	7.19	228.15	228.65	1.00	0.0413	0.0036	0.0547	0.0052	0.0095	0.000199	0.002437	0.000222	54.1	5.0	61.2	1.3	49.2	4.5
-26	3.27	106.67	135.01	0.79	0.0531	0.0071	0.0695	0.0091	0.0097	0.000338	0.002551	0.000303	68.2	8.7	62.3	2.2	51.5	6.1
-29	4.68	192.33	192.82	1.00	0.0425	0.0049	0.0560	0.0062	0.0098	0.000316	0.002753	0.000329	55.3	6.0	63.0	2.0	55.6	6.6
-31	7.59	265.64	241.34	1.10	0.0632	0.0081	0.0811	0.0099	0.0096	0.000308	0.003019	0.000339	79.1	9.3	61.5	2.0	60.9	6.8
-32	5.49	174.37	134.20	1.30	0.0480	0.0052	0.0638	0.0064	0.0098	0.000291	0.003491	0.000353	62.8	6.1	62.9	1.9	70.4	7.1
-33	7.80	280.18	225.00	1.25	0.0593	0.0066	0.0754	0.0080	0.0094	0.000334	0.002963	0.000233	73.8	7.6	60.2	2.1	59.8	4.7
-34	12.44	342.75	301.10	1.14	0.0481	0.0047	0.0638	0.0063	0.0097	0.000277	0.003302	0.000281	62.8	6.0	62.2	1.8	66.6	5.7

-35	4.65	139.54	145.58	0.96	0.0483	0.0050	0.0616	0.0064	0.0094	0.000255	0.003053	0.000348	60.7	6.1	60.1	1.6	61.6	7.0
-36	3.87	122.63	147.96	0.83	0.0544	0.0074	0.0684	0.0085	0.0096	0.000334	0.002782	0.000336	67.1	8.1	61.4	2.1	56.1	6.8
-37	3.14	98.17	90.77	1.08	0.0406	0.0081	0.0544	0.0098	0.0100	0.000469	0.002702	0.000308	53.8	9.5	63.8	3.0	54.5	6.2
BN5208-1	granite E：85°00′00"，N：30°27′57"																	
-1	5.62	188.70	239.64	0.79	0.0483	0.0037	0.0645	0.0050	0.0097	0.000203	0.002674	0.000210	63.4	4.8	62.2	1.3	54.0	4.2
-3	5.06	195.34	241.72	0.81	0.0538	0.0057	0.0675	0.0060	0.0094	0.000183	0.002220	0.000172	66.3	5.8	60.1	1.2	44.8	3.5
-5	6.16	231.75	278.59	0.83	0.0543	0.0051	0.0706	0.0068	0.0093	0.000262	0.002355	0.000241	69.3	6.5	60.0	1.7	47.5	4.9
-6	5.86	211.22	258.73	0.82	0.0566	0.0086	0.0745	0.0117	0.0096	0.000286	0.002400	0.000295	73.0	11.1	61.3	1.8	48.5	6.0
-7	4.75	183.47	217.38	0.84	0.0474	0.0047	0.0623	0.0065	0.0095	0.000418	0.002241	0.000359	61.4	6.2	61.3	2.7	45.2	7.2
-8	4.92	184.69	229.50	0.80	0.0490	0.0053	0.0621	0.0058	0.0094	0.000216	0.002351	0.000223	61.2	5.6	60.3	1.4	47.5	4.5
-9	6.38	212.07	264.27	0.80	0.0508	0.0039	0.0685	0.0051	0.0098	0.000253	0.002719	0.000202	67.3	4.9	63.0	1.6	54.9	4.1
-11	5.01	246.16	336.57	0.73	0.0560	0.0033	0.0739	0.0044	0.0097	0.000214	0.002930	0.000145	72.4	4.2	62.1	1.4	59.1	2.9
-13	5.84	255.07	388.45	0.66	0.0563	0.0036	0.0735	0.0044	0.0097	0.000187	0.003367	0.000154	72.0	4.1	62.3	1.2	67.9	3.1
-15	3.80	184.34	283.21	0.65	0.0609	0.0046	0.0758	0.0051	0.0096	0.000251	0.003191	0.000166	74.2	4.8	61.8	1.6	64.4	3.3
-16	4.59	212.73	326.45	0.65	0.0577	0.0038	0.0775	0.0047	0.0098	0.000216	0.003294	0.000168	75.8	4.5	63.1	1.4	66.5	3.4
-17	4.86	196.76	333.04	0.59	0.0565	0.0053	0.0759	0.0067	0.0101	0.000271	0.003415	0.000227	74.3	6.4	64.5	1.7	68.9	4.6
-18	4.96	244.76	294.28	0.83	0.0590	0.0045	0.0782	0.0058	0.0101	0.000281	0.003649	0.000169	76.4	5.5	64.7	1.8	73.6	3.4
19	4.23	196.54	295.12	0.67	0.0556	0.0047	0.0715	0.0060	0.0096	0.000326	0.003424	0.000227	70.1	5.7	61.3	2.1	69.1	4.6
-20	3.82	175.49	266.89	0.66	0.0578	0.0052	0.0758	0.0069	0.0098	0.000308	0.003321	0.000201	74.1	6.5	63.1	2.0	67.0	4.1
-21	7.54	443.54	397.17	1.12	0.0572	0.0051	0.0761	0.0063	0.0100	0.000282	0.003616	0.000165	74.5	6.0	64.1	1.8	73.0	3.3
-22	4.50	226.43	322.73	0.70	0.0587	0.0049	0.0725	0.0048	0.0096	0.000259	0.003150	0.000180	71.0	4.5	61.7	1.7	63.6	3.6
-23	4.65	202.77	310.82	0.65	0.0577	0.0042	0.0775	0.0059	0.0099	0.000265	0.003418	0.000292	75.8	5.6	63.2	1.7	69.0	5.9
-24	6.05	220.12	484.42	0.45	0.0539	0.0034	0.0711	0.0040	0.0101	0.000236	0.003146	0.000164	69.8	3.8	64.5	1.5	63.5	3.3
-25	3.66	94.51	336.00	0.28	0.0566	0.0041	0.0720	0.0046	0.0096	0.000253	0.003222	0.000257	70.6	4.4	61.7	1.6	65.0	5.2
-26	3.57	158.55	272.30	0.58	0.0516	0.0047	0.0658	0.0055	0.0097	0.000226	0.003358	0.000223	64.7	5.2	62.0	1.4	67.8	4.5
-27	3.39	171.63	267.28	0.64	0.0588	0.0059	0.0699	0.0060	0.0096	0.000328	0.003000	0.000196	68.6	5.7	61.3	2.1	60.5	4.0

5 Discussion

5.1 Age of rock formation

Nuocang area granite porphyry (BN4405-Dy) and granite samples (BN5208-1) have weighted mean ages of 61.86±0.8 Ma and 62.17±0.67 Ma, respectively, suggesting that a latest emplacement starting date for Paleocene granitoids at 61.86 ± 0.8 Ma, in the Paleocene. The Dianzhong Formation's basaltic andesitic crystal tuff interlayer is also present in the Nuocang area. According to previous research, the Dianzhong Formation formed in the western Gangdese belt 51.6-64.8 Ma in the Dajiacuo area (Geological Survey of Jiangxi Province., 2015), 61-63.9 Ma in the Coqen area (Hu et al., 2007), 58.55-60.07 Ma in the Coqen-Angren area (Wen et al., 2008) and, by its olivine theoleiite formation, 58.4-60.1 Ma in the Shiquanhe area. To sum up, the basaltic andesitic crystal tuff is likely to have formed 60 Ma, which corresponds to the formation age of granites in the study area. Previous studies have shown that the India-Eurasia collision was simultaneously in eastern and western directions, with initial collision occurring 65Ma (Hou et al., 2006, Mo et al., 2007; Dong et al., 2011). The Linzizong Formation volcanic rocks represent the initial collision tectonic environment, and its formation age likewise corresponds to the granitoids in this study. Meanwhile, evidence of large-scale magmatic activity in the Paleocene has been found in the Gangdese Belt (Table 4). In simultaneity, the Linzhou basin developed intermediate-acid dykes (55.1-62 Ma (Dong et al., 2017)), Riduo granite and granodiorite porphyrite (59.5-62.7Ma, (Wang et al., 2019)), Zhula Bi-monzogranite mass (63-64 Ma; Li et al 2012) and basic dikes found Near Lhasa (60 Ma, (Lü et al. 2012)), Nanmulin (62.4 Ma,(Zhu et al. 2011)) and Xiongga (64.7 Ma, (Chen et al. 2017)), respectively. Additional data on the western Gangdese Belt's Dianzhongzu Formation granite porphyry (62 Ma, (Jiang, 2018)) and basic volcanic rocks of the Shiquanhe area (60.1 Ma, (Tibet Geological Suvery Institute, 2003)) indicate simultaneous magmatic activity. It is worth mentioning that the Dianzhong Formation's intermediate-acid volcanic rocks and contemporaneous intermediate-acid intrusive rocks of the eastern and western Gangdese Belt exhibit strong geochemical similarities—in terms of components, peraluminosity, calc-alkaline classification, trace element enrichment or depletion, and a right-leaning REE

284 distribution.

285 Therefore, Nuocang Paleocene granitoids and basaltic andesitic crystal tuff are Paleocene

286 magmatic events under the influence of the initial continental collision between India and Eurasia.

287

288 Table 4. Gangdese Paleocene magmatic rocks: locations and ages

Structural location	Number	Sample	Locality	Longtitude(°E)	Latitude(°N)	Rock type	Age (Ma)	Ref.
	1	LZ1104	Linzhou basin	91°01. 9' – 91°11.9	29°54. 9' – 29°58. 2'	granite porphyry	55. 1	Dong *et al.* 2015
	2	LZ1106	Linzhou basin	91°01. 9' – 91°11.9	29°54. 9' – N29°58. 2'	granite porphyry	57. 8	Dong *et al.* 2015
	3	LZ1110	Linzhou basin	91°01. 9' – 91°11.9	29°54. 9' – 29°58. 2'	granite porphyry	61. 1	Dong *et al.* 2015
	4	LZ1113	Linzhou basin	91°01. 9' – E91°11.9	29°54. 9' – N29°58. 2'	granite porphyry	59. 8	Dong *et al.* 2015
	5	LZ1108	Linzhou basin	91°01. 9' – E91°11.9	29°54. 9' – 29°58. 2'	Bi-granodiorite porphyrite	62. 4	Dong *et al.* 2015
	6	NML03-1	Nanmulin			Diorite	62.4	Zhu *et al.* 2011
	7	2003T363	Linzhou basin			trachybasalt	52.54	Yue *et al.* 2006
	8	2003T363	Linzhou basin			trachybasalt	52.9	Yue *et al.* 2006
	9	BLZ-02	Linzhou basin			granite porphyry	60.3	Wang *et al.* 2006
	10	T0889-D	Riduo			granodiorite porphyrite	62.7	Wang *et al.* 2019
	11	T0889-G	Riduo			granite	59.5	Wang *et al.* 2019
Eastern Gangdese	12	G07a	Zhula	93°18′ 00″ -93°53′ 40″	30°01′22″-30°11′08″	Bi-monzogranite	63.9	Li *et al.* 2012
	13	G01	Zhula	93°18′00″-93°53′40″	30°01′22″-30°11′08″	Bi-monzogranite	64.6	Li *et al.* 2012
	14	G03a	Zhula	93°18′00″-93°53′40″	30°01′22″-30°11′08″	Bi-monzogranite	64.3	Li *et al.* 2012
	15	XM-1	around Lhasa	92.20°	29.71°	Bi-Q-diorite	64	Lü *et al.* 2012
	16	XM-2	around Lhasa	92.10°	29.70°	Bi-Q-diorite	65.9	Lü *et al.* 2012
	17	XM-3	around Lhasa	92.08°	29.71°	Granite	67.2	Lü *et al.* 2012
	18	XM-4-2	around Lhasa	92.04°	29.72°	Monzogranite	66.6	Lü *et al.* 2012
	19	XM-5	around Lhasa	91.98°	29.73°	Bi-monzogranite	67.5	Lü *et al.* 2012
	20	XM-6	around Lhasa	91.96°	29.74°	Monzogranite	68.7	Lü *et al.* 2012
	21	XM-7	around Lhasa	91.20°	29.63°	Bi-granodiorite	60.3	Lü *et al.* 2012
	22	XM-8	around Lhasa	91.20°	29.64°	Bi-granodiorite	58.2	Lü *et al.* 2012
	23	XM-9	around Lhasa	91.16°	29.72°	Bi-monzogranite	57.6	Lü *et al.* 2012

	24	XM-16	around Lhasa	92.10 °	29.71 °	Diorite-vein	60	Lü *et al.* 2012
	25	XM-17	around Lhasa	92.10 °	29.71 °	Monzogranite	68.4	Lü *et al.* 2012
	26	XG-12-2	Xiongga	91.71 °	29.27 °	Quartzmonzonite	64.77	Chen *et al.* 2017
	27	XG-12-3	Xiongga	91.71 °	29.27 °	Gabbro	64.77	Chen *et al.* 2017
	28		Shiquanhe			olivine tholeiite	60.1	1:250000Shiquanhe regional report. 2003
	29		Shiquanhe			olivine tholeiite	58.4	
Western Gangdese	30	BN0207	Beina	86°12′30″～86°14′00″	30°05′30″～30°07′00″	granite porphyry	63.2	Jiang 2018
	31	BN02	Beina	86°12′30″～86°14′00″	30°05′30″～30°07′00″	granite porphyry	63.3	Jiang 2018
	32	P3308H1	Coqen			andesite	61	Hu *et al.* 2011
	33	BN4405-DY	Nuocang	85°09′10"	30°24′03"	granite porphyry	61.8	This study
	34	BN5208-1	Nuocang	85°00′00"，	30°27′57"	granite porphyry	62.17	This study

289

5.2 Tectonic implications

According to Zircon U-Pb dating, granitiods in this study formed in the same basic timeframe as the India-Eurasia continental collision, matching the age of collision-related granite porphyry samples from the eastern Gangdese Belt. They also conform to the eastern Gangdese Belt in terms of major and trace elements, major element content, enrichments of large ion lithophile elements (LILE) (e.g., K, Rb, Ba, Th, and U), and depletions in high field-strength elements (HFSE) (e.g., Nb, P, and Ti)—all these signs of subduction-related igneous activity (Pearce et al., 1984; Condie, 2001; Mo et al., 2003). However, when comparing collision-related granite porphyry with $J_{1\text{-}2}$-K typical subduction arc volcanic rocks (Yeba Formation and Sangri group) and Miocene (10~18 Ma) adakitic granite porphyry from the post-collision crustal extension environment, (Wang et al., 2006) found that the Paleocene granite porphyry belonged neither to adakitic nor subduction volcanic rock types. Instead, it should be concluded as intracontinental magmatism transforming from subduction to collision.

The Dianzhong Formation developed a layer of basaltic-andesite in the Gangdese belt. The widespread manifestation of mafic/ultramafic magmatism can be regarded as a collisional thickening environment (S.V. Khromykh and A.G. Vladimirov., 2013). In addition, an analysis of the volcanic geochemistry of the Dianzhong Formation signifies the extent of crustal material impact on the magma. In particular, the appearance of shoshonite series in the Nianbo and Pana Formations is a strong indicator of intracontinental magmatism (Mo., 2003; Dong et al., 2015). Nuocang granites samples can almost classify as high-K calc-alkaline, very close to the shoshonite series, implying that the area formed under an initial collision environment.

5.3. Petrogenesis

Granite is generally believed to be formed by the partial melting of crustal materials, while crustal composition is itself highly heterogeneous. The melting source area may not be pure igneous or pure sedimentary rock. The material heterogeneity of the source area may be inherited by molten magma and even retained in the final crystallized rocks (Wang et al., 2017; Zheng et al., 2019). Zircon Hf isotope analysis is widely used to study granite rock source properties and

characteristics. Positive values of $\varepsilon_{Hf}(t)$ are generally interpreted as juvenile crust melting or the addition of mantle materials, while granites with negative $\varepsilon_{Hf}(t)$ values are thought to originate from ancient crustal materials (Taylor and McClenna., 1985; Wu et al., 2007). Zircon Hf isotope analysis of Nuocang Paleocene granite suggests a compositionally uniform source material. The value of $\varepsilon_{Hf}(t)$ ranges from -7.63 to -3.36, with the t_{DM}^{C} age of 1.4-1.6 Ga, indicative of ancient crustal material(Fig.8). A large variation in $\varepsilon_{Hf}(t)$ values requires an open system to change the ratio of $^{176}Hf/^{177}Hf$ in the melt (Kemp et al.,2007). Because the zircon Hf isotope ratio not change with partial melting or fractional crystallization, the heterogeneity of zircon Hf isotopes probably indicates interaction between the more radiogenic Hf mantle provenance and the less radiogenic Hf crustal materials (Bolhar et al., 2008). Granitoids in this study had negative $\varepsilon_{Hf}(t)$ values, in this respect clearly diverging from eastern Gangdese Belt granitoids. This contradicts previous conclusions that the southern margin of the Gangdese belt formed from juvenile crust. Some scholars believe this to be the result of ancient crustal melt in the India continent (Dong et al., 2017). But most believe that the Southern Lhasa Block has an ancient crystalline basement (~84~88°E) (Hou et al., 2015; Zhang et al., 2018; Jiang, 2018). Mo et al (2006, 2009) According to the post-collision potassic-superpotassic volcanic rocks of the Miocene (8-25 Ma), it is speculated that it mainly formed by breaking off the Neo-Tethys plate during the post-collision stage.Then the Indian continental lithosphere subducted to the bottom of the Lhasa Terrane. Therefore, it can be preliminarily concluded that the Indian contintental lithosphere did not subduct below the Lhasa terrane at least before 25 Ma. The discrepancy in eastern and western Gangdese Belt granitoid samples' $\varepsilon_{Hf}(t)$ values may be mainly caused by differences in their crystalline basements.

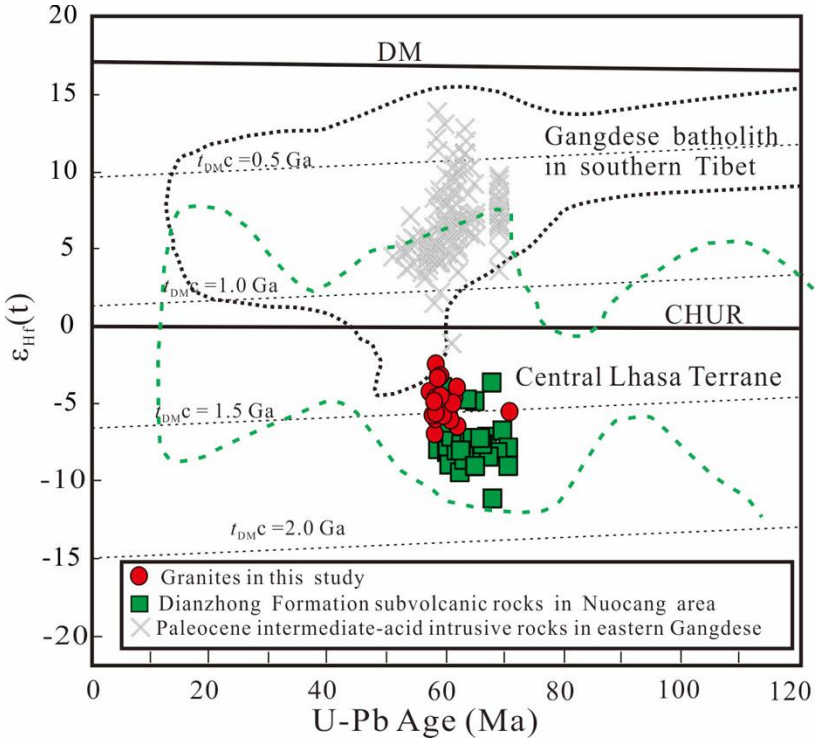

Fig.8 Gangdese Nuocang granitoid and Paleocene granite $\varepsilon_{Hf}(t)$ values Gangdese batholith data from Ji et al.,(2012); Nuocang area Dianzhong Formation subvolcanics data from (Jiang, 2018); eastern Gangdese Paleocene intermediate intrusives from Dong *et al.* (2017); Wang *et al.* (2006); Lü*et al.* (2012)

According to the standardized distribution diagram of REE chondrites for Nuocang granitoids, 11 samples have obvious negative δEu anomalies. Negative δEu anomalies are generally explained in two ways: either in relation to the fractional crystallization of plagioclase in magma, or in relation to the existence of a refractory residual phase during partial melting of the crustal source area (Rollison, 1993). However, the thickness of Linzizong Group volcanics in the Coqen basin exceeds 2800m (Ding et al., 2017) and they are widely distributed across the Gangdese Belt. With such a wide distribution, it becomes difficult to explain the formation of Nuocang granitoids in the relatively short timeframe proposed by magmatic fractionation. Therefore, the melting of continental crust may have played a more important role during formation (Dong et al., 2005, 2008; Mo et al., 2009; Dong et al., 2015).

In addition, Nuocang granite porphyry is relatively enriched with large ion lithophile elements (LILE) (e.g., K, Rb, Ba, Th, and U) and deficient in high field-strength elements (HFSE) (e.g., Nb, P, and Ti) (Fig 8b). On the one hand, the loss of high field strength elements may reflect source rock properties, because crustal melts are typically characterized by a loss of high field

strength elements (Ryerson et al., 1987; Xie et al, 2013); on the other hand, a relatively high loss of Nb, P and Ti suggests the possible fractionation and crystallization of Ti-rich minerals—since Ti is not easily combinable and remains in the source area. P deficit, meanwhile, is caused by apatite separation and crystallization during magmatic evolution and fractionation (Rollison, 1993; Wu et al., 2003).

On Nb-Nb/Th diagrams (Fig. 9a), most of the samples are close to continental crust, and far from the primitive mantle and MORB regions, with the same geochemical properties as volcanic arc rocks. On Nb/Y-Th/Y diagrams (Fig. 9b), most samples fall far from the upper crust but rather between Th/Nb = 1 and Th/Nb = 10 trend lines, close to the average composition of the lower and mid-crust. In addition, the samples' La/Nb ratios ranged from 3.8 to 10.7, with an average value of 5.8, far greater than 1.0 and thus differing from mantle-derived magma (De Paolo and Daley., 2000). The samples' low MgO content (Table 3) likewise implies that area granitoids are derived from the partial melting of crustal materials.

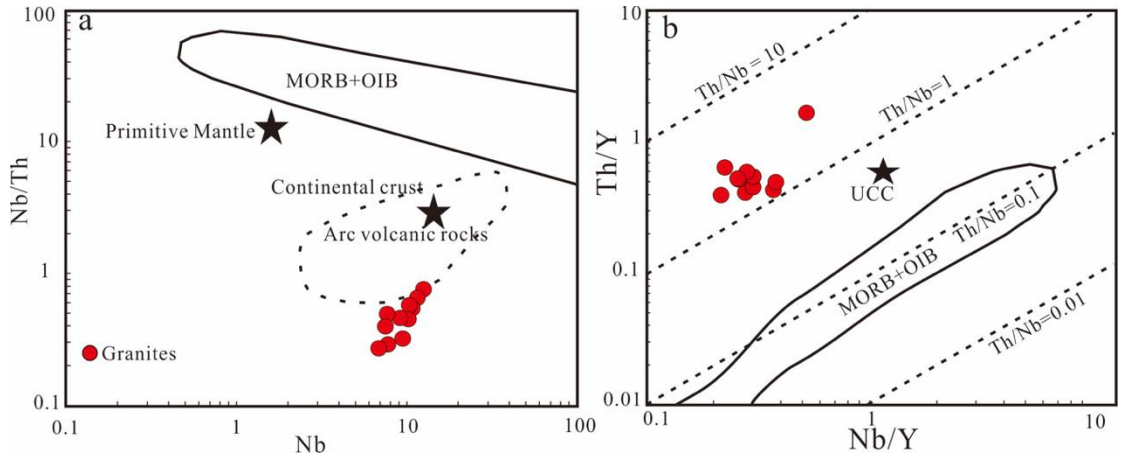

Fig. 9 Nb vs. Nb/Th (a) and Nb/Y vs. Th/Y (b) discrimination diagrams (*as in* Boztu et al.，2007). Data sources: primitive mantle (Hofmann, 1988); continental crust, MORB, OIB, and arc volcanic rock (Schmidberger and Hegner, 1999)

From the La-La/Yb diagram (Fig. 10a), we see that the slope of the distribution curve of Paleocene granites in the Nuocang area lies closer to the partial melting line. Partial melting may be the main controlling factor in magma genesis.

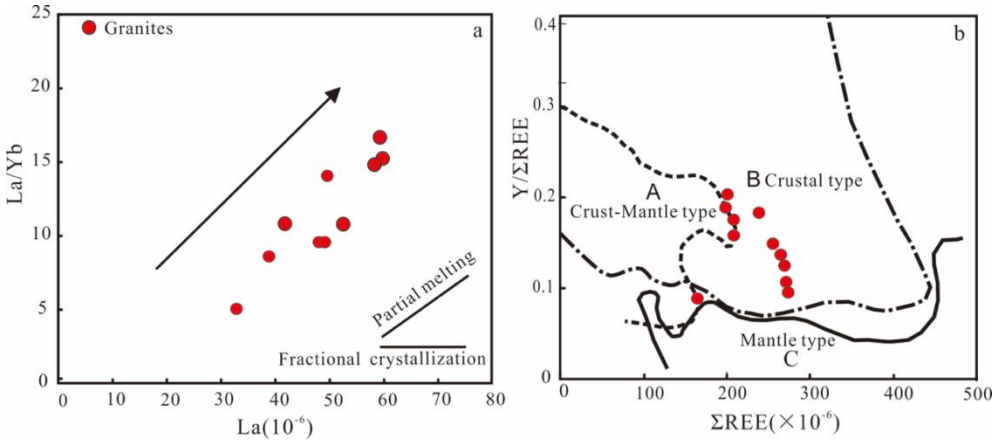

Fig10 La vs. La/Yb diagram (a) and ΣREE vs. Y/ΣEREE diagram (b) (*as in* Lü et al., 1993). A-crust-mantle type granite ; B-crust-type granite ; C-mantle-type granite

Granites in this study are thus believed to be formed primarily by the partial melting of crustal materials, where crustal composition is heterogeneous. That is, the melting source may not be pure igneous or pure sedimentary rock. This material heterogeneity of the source may have been inherited into the magma and retained in the resulting crystallized rocks (Wang et al., 2017, Zheng et al., 2019). In the ΣREE-Y/ΣREE diagram, all samples fall into the crustal source area (Fig. 10b), indicating main derivation from partial melting of the lower crust. Comparison of geochemical composition between these granitoids and the experimental melt shows an even source material composition. Source rocks may include only the ancient crust, dominated by metagreywackes (Figs. 11a), which is consistent with zircon Hf isotope analysis results, which also suggest an even source material composition.

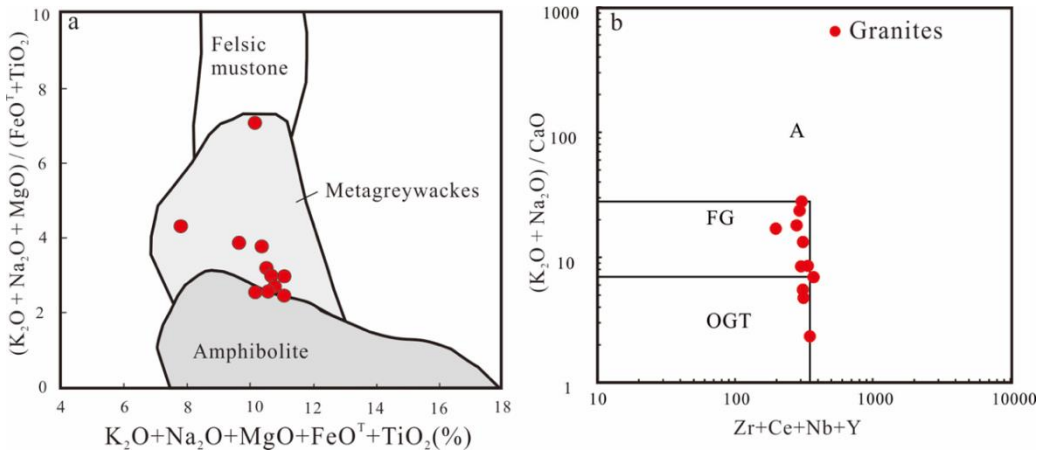

Fig.11. Geochemical diagrams of $K_2O+Na_2O+MgO+FeO^T+TiO_2$ vs. $(K_2O+Na_2O)/(MgO+FeO^T+TiO_2)$ and $(K_2O+Na_2O/CaO$ vs. Zr+Nb+Ce+Y （a, Whalen et al.(1987)）for the Paleocene granitoids (b, after Kaygusuz et al., 2008)

It is generally recognized that the magma originated from melting of the lower crust materials $Mg^{\#}<40$ (Atherton and petford,1993) and the partial melting of basalt $Mg^{\#}>45$ (Rapp,1997). More basic materials than basalt mixed with $Mg^{\#}>50$ (Wu et al.,2003) and direct partial melting of mantle peridotite $Mg^{\#}>60$ (McCarron and Smell-ie, 1998). The $Mg^{\#}$ value of basic rock samples ranges from 47 to 52, with a mean of 50, indicating that the source is not completely crustal, but may have mantle-derived materials mixed in. The La/Yb vs. Sm/Yb diagram shows that possibly 10% of garnet-peridotite in the basaltic andesitic crystal tuff was partially melted (Fig. 12a) and contaminated by crust during upward emplacement (Fig. 12b) .

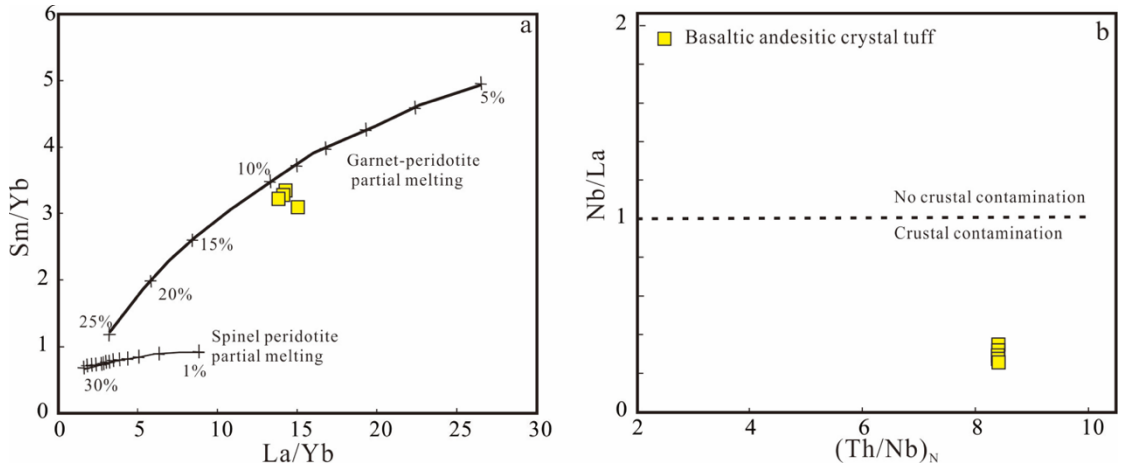

Fig. 12 Plot of La/Yb vs. Sm/Yb (a, after Johnson et al., 1990) and plot of $(Th/Nb)_N$ vs. Nb/La (b, after Kieffer et al., 2004; normalized values from Sun and McDonough, 1989, for Nuocang area basaltic andesitic crystal tuff samples

5.4 Dynamic Evolution

Prior to India-Eurasia continental collision, the Neo-Tethys oceanic lithosphere subducted beneath the Eurasian continent at a normal angle to form typical epicontinental arc volcanic rocks (~120-65Ma. Then, initial plate collision occurred 65Ma. Under the influence of gravity, the Neo-Tethys oceanic lithosphere subducted deeply and rotated in the process. Near the Moho surface, partial melting of the hydrated mantle wedge generated magma upwelling. The intense heat melted ancient Lhasa crust along with a portion of the mantle-derived magma, resulting in a wide area of highly differentiated acidic volcanic rock formation—that is, the Linzizong Formation. As the Neo-Tethys Lithosphere continued subducting, the Indian plate pushed below the Eurasia

plate. The lifting of the subduction zone resulted in an environment of crustal extension and thinning. Crustal decompression, mantle thermal upwelling, and partial melting together produced the basic volcanic interlayer of the Dianzhong Formation.

6 Conclusions

1) Nuocang granite and granite porphyry yield ages of 61.86 ± 0.8 Ma（MSWD = 0.6）and 62.17±0.67 Ma(MSWD = 0.052) respectively, indicating that these intrusions formed in the early Paleocene. This concurs with the formation ages of east Gangdese Belt granitoids, likely indicating that early Paleocene magmatic activity in the Gangdese Belt was synchronous from east to west.

2) Nuocang granites are calc-alkaline to high-K calc-alkaline and metaluminous to peraluminous with a high DI index and a right-leaning REE pattern. They feature enrichments of incompatible elements and LILE—such as Rb, Ba, Th, and K—along with pronounced depletions of high field elements (HFSE)—such as Nb, Sr, Ti, and P.

3) The granitoids' source is derived from the melting of ancient crystalline basement metagreywackes; its basaltic andesitic crystal tuff is derived from the partial melting of garnet-peridotite partial melting and crustal contamination occurred during the intrusion of upwelling magma .

We thank N.L. Dobretsov and A E.lzokh for useful discussion.

1:50,000 regional geological survey projects of the Luocang area were mainly undertaken at Chengdu University of Technology. The Level 2 project uses the Gangdese metallogenic belt base survey items (project code: 1212011221067) and is supported by Central funding. My sincere thanks extend to the members of the Luocang project for their help in the field and their constructive comments and suggestions.

References

Atherton,M.p, Petoord,N.,1993. Generation of Sodium-Rich Magmas from Newly Underplated Basaltic Crust. Nature, 362(6416)，144-146.

Bao, CH., Ding, F., Wang, Q., Liu, SH., Xu, F., He, CX., 2014. Lithochemical, geochemical, characteristics and

tectonic setting of the volcanic rocks in the Eocene Pana Formation, Linzizong Group, in the Xiongma area, Coqen County, Xizang (Tibet). Geological Review. 60(2): 275-284() (in Chinese with English abstract).

Bolhar, R., Weaver, S., 2008. White house Metal,Sources and Evolution of Arc Magmas Inferred from Coupled O and Hf Isotope Systematics of Plutonic Zircon s from the Cretaceous Separation Point Suite (New Zea-land). Earth and Planetary Science Letters

Chu, MF., Chung, SL., O'Reilly, SY., Pearson, NJ., Wu, FY., Li, XH., Liu, DY., Ji, JQ., Chu, CH., Lee, HY.. 2011. "India's hidden inputs to Tibetan orogeny revealed by Hf isotopes of Transhimalayan zircons and host rocks". Earth and Planetary Science Letters.307 (3-4): 479-486.

Chung, SL., Liu, DY., Ji, JQ., Chu, MF., Lee, HY., Wen, DJ., Lo, CH., Lee, TY., Qian, Q., Zhang, Q., 2003.Adakites from continental collision zones: Melting of thickened lower crust beneath southern Tibet. Geology, 31(11): 1021-1024.

Condie, KC., 2001. Mantle plume and their record in earth history. London: Cambridge University Press,

Dobretsov, N.L., 2008. Geological implications of the thermochemical plume model. Russian Geology and Geophysics (Geologiya i Geofizika) 49 (7),441–454 (587–604).

Dobretsov, N.L., Buslov, M.M., 2011. Problems of geodynamics, tectonics, and metallogeny of orogens. Russian Geology and Geophysics (Geologiyai Geofizika) 52 (12), 1505–1515 (1911–1926).

Dobretsov, N.L., Borisenko, A.S., Izokh, A.E., Zhmodik, S.M., 2010. A thermochemical model of Eurasian Permo-Triassic mantle plumes as a basis for prediction and exploration for Cu-Ni-PGE and rare-metal ore deposits. Russian Geology and Geophysics (Geologiya i Geofizika) 51 (9), 903–924 (1159–1187).

Ding, Feng., Xu, Zhongbiao., Liu, Shouhang., Li, Yue., Gao, Jianguo., Fan, Yuhang., Li, Qing., 2017. LA-ICP-MS Zircon U-Pb Ages, Petrochemical Characteristics and Petrogenesis of the Volcanic Rocks from the palaeocene—Eocene Nianbo Formation in Chima Area, Coqen County, Xizang(Tibet). 63(4):1102-1116

Dong, GC., Mo, XX.,Zhao, ZD., Zhu, DC., Xie, XF., Dong, ML., 2011. The Neocene magmatism from Namuru intrusion in western Gangdese,Tibet and its tectonic significance. Acta Petrologica Sinica.27(7): 1983-1992

Dong, MC., Zhao, ZD., Zhu, DC., Liu, D., Dong, GC., Mo, XX., Hu, ZC., Liu, YS., Zou, ZH., 2015. Geochronology, geochemistry, and petrogenesis of the intermediate and acid dykes in Linzhou Basin, southern Tibet. Acta Petrologica Sinica 31(5), 1268-1284.

Fei, GC., Zhao, FM., Xu, JB., Li, YG., 2014. Geochemical characteristics and its Geological implications of madeng vocanic Rocks in Anduo, North Tibet. Mineral petro l34(1), 46-51.

Stupak, F M., Yarmolyuk, V V., KUdryashova, EA., 2020. Late Mesozoic volcanism in the UST"-KARA basin

(eastern Transbaikalia) and its relationship with magmatism of the great Xing An and East Mongolian volcanic belts. Russian Geology and Geophysics. Nos. 5-6.

Guo, Z F., Wilson, M., Liu, J Q., 2007. Post-collisional adakites in south Tibet: Products of partial melting of subduction-modified lower crust. Lithos 96, 205–224.

Guo, Z F., Wilson, M., Zhang, M L., Cheng, Z H., Zhang, L H., 2013. Post-collisional, K-rich mafic magmatism in south Tibet: Constraints on Indian slab-to-wedge transport processes and plateau uplift. Contributions to Mineralogy and Petrology 165, 1311–1340.

Hoskin, PWO., Schaltegger, U., 2003. The composition of zircon andigneous and metamorphic petrogenesis, In: Manchar JM and HoskinPWO (eds). Zircon. Reviews of Mineralogy and Geochemistry53(1), 27-62.

Hou, ZQ., Wang, EQ., Mo, XX., Ding, L., Pan, GT., Zhang, ZJ., 2008. Collisional Orogeny and Metallogenesis of the Tibetan Plateau.Beijing: Geological Publishing House,1-980. (in Chinese)

Hu, Xin-wei., MA, Run-ze., TAO, Xiao-feng., LIU, Deng-zhong., 2007 .SHI He Lithogeochemical characteristics and tectonic setting of volcanic rocks of Dianzhong Formation in the Coqen area, Tibet, China 33(1),15-21.

Hu, XM., Garzanti, E.,Wang, JG., Huang, WT.,An, W., Webb, A., 2016.The timing of India-Asia collision onset: Facts, theories, controversies. Earth-Science Reviews160, 264-299.Chayka, Van. F., Liudmila M, Zhitova., Tatiana N, Antsiferova., Adam, Abersteiner., Artem, Ya., Shevko, Andrey E, Izokh., Nadezhda, D., Tolstykh, Marina P., Gora Valery M, Chubarov.,Vadim S, Kamenetsky. 2020. In-Situ Crystallization and Continuous Modification of Chromian Spinel in the “Sulfide-Poor Platinum-Group Metal Ores” of the Norilsk-1 Intrusion (Northern Siberia, Russia). Minerals10(6), 498.

Ji, W Q., Wu, F Y., Chung, S L., Li, J X., Liu, C Z., 2009. Zircon U-Pb geochronology and Hf isotopic constraints on petrogenesis of the Gangdese batholith, southern Tibet. Chemical Geology 262, 229–245.

Ji, W Q., Wu, F Y., Liu, C Z., Chung, S L., 2012. Early Eocene crustal thickening in southern Tibet: New age and geochemical constraints from the Gangdese batholith. Journal of Asian Earth Sciences 53, 82-95.

Ji, WQ., Wu, FY., Chung, SL., Liu, CZ., “Geochronology and petrogenesis of granitic rocks in Gangdese batholith，southern Tibet.”.Science in China (Series D) 52(9), 1240-1261(2009b).

Kemp, A., Hawkesworth, C., Foster, G., 2007.Magmatic and Crustal Differention History of Granitic Rocks from Hf-O Istopes in Zircon. Science 315, (5814): 980-983.

Lee, H Y., Chung, S L., Ji, J Q., Qian, Q., Gallet, S., Lo, C H., Lee, T Y., Zhang, Q., 2011. Geochemical and Sr-Nd isotopic constraints on the genesis of the Cenozoic Linzizong volcanic successions, southern Tibet. Journal of Asian Earth Sciences 53, 96–114...

Lee, H Y., Chung, S L., Lo, CH., Ji, J Q., Lee, T Y., Qian, Q., Zhang, Q., 2009. Eocene Neotethyan slab breakoff in southern Tibet inferred from the Linzizong volcanic record. Tectonophysics 477, 20-35.

Li, C., 1987. The Longmucuo-Shuanghu-Lancangjiang plate suture and thenorth boundary of distribution of Gondwana facies Permo-Carboniferous system in northern Xizang, China. Journal of Changchun College of Geology 17(2), 155-166. (in Chinese with English abstract)

LI, Yue., DING, Feng., LIN, Jichun., LIU, Shouhang., XU, Zhongbiao., WEI, Meili., LI, Qing., GAO, Jianguo., FAN, Yuhang., QIU, Xiong., 2017. LA-ICP-MS Zircon U-Pb Ages and Geochemical Characteristicsof Tajilixialong Granodiorite in Nuocang Area,Coqen,Xizang(Tibet) 63(2), 484-498.

LI, Zai-hui., ZHENG, Lai-lin., LI, Jun-min., XIA, Xiang-biao., 2009.^{40}Ar-^{39}Ar Dating of Linzizong Volcanic Rocks in the CentralGangdise Area and Its Geological Implication 28(3), 223-228

Liu, Y.G., Chen, Z.G., Li, W.Y., Xu, X.H., Kou, X., Jia, Q.Z., Zhang, Z.W., Liu, F., Wang, Y.L. You, M.X., 2019. The Cu-Ni mineralization potential of the Kaimuqi mafic-ultramafic complex and the indicators for the magmatic Cu-Ni sulfide deposit exploration in the East Kunlun Orogenic Belt, Northern Qinghai-Tibet Plateau, China. Journal of Geochemical Exploration 198, 41-53.

Li, MinZhou., Wang, Rui., Hou, Zengqian. Li,Chao., Zhao, Hong., Li,Xin-Wei., Qu,Wen-Jun.,2018. Hot Paleocene-Eocene Gangdese arc: Growth of continental crust insouthern Tibet. Gondwana Research 62,178-197.Liu, Y.G., Li, W.Y., Jia, Q.Z., Zhang, Z.W., Wang, Z.A., Zhang, Z.B., Zhang, J.W. Qian, B., 2018. The Dynamic Sulfide Saturation Process and a Possible Slab Break-off Model for the Giant Xiarihamu Magmatic Nickel Ore Deposit in the East Kunlun Orogenic Belt, Northern Qinghai-Tibet Plateau, China. Economic Geology 113(6), 1383-1417.

LÜ, Xin., WANG, Zhenghua.,LIU,Yulin.,LIU, Hongfei., XU, Kaifeng., ZHANG, Jinshu.,2015. Geochronology and Geochemistry of the Late Cretaceousto Paleocene Intrusions in East Gangdese, Lhasa, Tibet and Their Tectonic Significances, ACTA GEOLOGICA SINICA (English Edition) 89(2),441-466.LUO, ZH., MO, XX., HOU, Zeng-Q., 2006. An integrated model for the Cenozoic evolution of the Tibetan plateau:constraints from igneous rocks. Earth Science Frontiers 13(4),196-211.

Ma, L., Wang, B D., Jiang, Z Q., Wang, Q., Li, Z X., Wyman, D A., Zhao, S R., Yang, J H., Gou, G N., Guo, H F., 2014. Petrogenesis of the Early Eocene adakitic rocks in theNapuri area, southern Lhasa: Partial melting ofthickened lower crust during slab break-off andimplications for crustal thickening in southern Tibet. Lithos, , 196–197 (321–338)

McCarron, J.J., 1998 Tectonic Implications of Fore-Arc Magmatism and generation of High Magnesian Andesites:

Alexander Island, Antarctia. Journal of the Geological Society 155(2),269-280.

Mo, X X., Zhao, Z D., Zhou, S., Dong, G C., Liao, Z L., 2007. On the timing of India-Asia continental collision. Geological Bulletin of China 26(10),1240- 1244

Mo, XX., Dong, GC., Zhao, ZD., Guo, TY., Wang, LL., Chen, T., 2005. Timing of magma mixing in the Gangdesê magmatic belt during the India-Asia collision: Zircon SHRIMP U-Pb dating. Acta Geologica Sinica 79(1), 66-76.

Mo, XX., Hou, ZQ.,Niu, YL., Dong, GC., Qu, XM., Zhao, ZD., Yang, ZM., 2007. Mantle contributions to crustal thickening during continentalcollision: Evidence from Cenozoic igneous rocks in southern Tibet.Lithos 96(1-2), 225-242.

Mo, XX., Niu, YL., Dong, GC., Zhao, ZD., Hou, ZQ., Zhou, S., Ke, S.,2008. “Contribution of syncollisional felsic magmatism to continentalcrust growth: A case study of the Paleogene Linzizong volcanic succession in southern Tibet”. Chemical Geology 250(1-4), 49-67.

MO, XX., PAN, GT., 2006. From the Tethys to the formation of the Qinghai-Tibet Plateau: constrained by tectono-magmatic events.Earth Science Frontiers 13(6) , 795-803.

Mo, XX., Zhao, ZD., Yu, XH., Dong, GC., Li, YG., Zhou, S., Liao, ZL., Zhu, DC., 2009. Cenozoic Collisional-Postcollisional Igneous Rocks in the Tibetan Plateau. Beijing: Geological Publishing House,1-396. [in Chinese]

Pan, GT., Mo, XX., Hou, ZQ., Zhu, DC., Wang, LQ., Li, GM., Zhao, ZD., Geng, QR., Liao, ZL., 2006. Spatial-temporal framework of the Gangdese orogenic belt and its evolution. Acta Petrologica Sinica22(3),521-533.[in Chinese with English Abstract]

Pearce Julian A, Harris Nigel BW and Tindle Andrew G. 1984. Trace element discrimination diagram for the tectonic interpretation of granitic rocks. Journal of Petrology , 25(4), 956-983

Qu, XM., Hou, ZQ., Mo, XX., Dong, GC., Xu, WY., Xin,HB., 2005. Relationship between Gangdese porphyry copper deposits and uplifting of southern Tibet plateau: Evidence from multistage zircon of ore_bearing porphyries. MINERAL DEPOSITS 25(4), 388-400.

Rapp, R. P., 1997. Heterogenous Source Regions for Archean Gran-itoids: Experimental and Geochemical Evidence.Oxford Monographs on Geology and Geophysics,35:267-279.

Rollison, HR., 1993. Using Geochemical Data: Evaluation, Presentation, Interpretation.London: Longman Group UK Ltd

Rowley, D B., 1996. Age of initiation of collision between India and A-sia: a review of stratigraphic data. Earth

564 Planet. Sci. Lett 145, 1-13.
565 Rowley, D B., 1998.Minimum age of initiation of collision between India and Asia north of the Everest based on
566 the subsidence history of the Zhe pure Mountain section. The Journal of Geology 106, 229- 235.
567 Searle, MP., Windley, BF.,Coward, MP., Cooper, DJW.,Rex, AJ., Rex, D., Li, TD., Xiao, XC., Jan, MQ., Thakur
568 V and Kumar S. 1987. The closing of Tethys and the tectonics of the Himalaya. Geological Society of
569 America Bulletin 98(6), 678-701.
570 Song, B., 2015. SHRIMP zircon U-Pb age measurement: Sample preparation, measurement, data processing and
571 explanation. Geological Bulletin of China 34(10), 1777-1788.
572 Sun, SS., McDonough, WF.,1989. Chemical and isotope systematics of oceanic basalts: Implications for mantle
573 composition and processes. In: Saunders AD and Norry MJ (eds). Magmatism in Ocean Basins Geological
574 Society, London, Special Publication 42 (1),313-345.
575 Sun, X., Zheng, YY., Xu, J., Huang, LH., Guo, F., Gao, SB., 2017. Metallogenesis and ore controls of Cenozoic
576 porphyry Mo deposits in the Gangdese Belt of southern Tibet. Ore Geology Reviews81, 996-1014.
577 Khromykh, S.V., Vladimirov, A.G., Izokh, A.E., Travin, A.V., Prokop'ev, I.R., Azimbaev, E., Lobanov, S.S.,
578 2013. Petrology and geochemistry of gabbro and picrites from the Altai collisional system of Hercynides:
579 evidence for the activity of the Tarim plume Russian Geology and Geophysics 54, 1288-1304.
580 Tang, JX., Lang, XH., Xie, FW., Gao, YM., Li, ZJ., Huang, Y., Ding, F., Yang, HH., Zhang, L., Wang, Q., Zhou,
581 Y., 2015. "Geological characteristics and genesis of the Jurassic No. I porphyry Cu-Au deposit in the
582 Xiongcun district, Gangdese porphyry copper belt,Tibet". Ore Geology Reviewsn 70, 438-456..
583 Taylor, SR., McClennan, SM., 1985. The Continental Crust ItsComposition and Evolution. Oxford: Blackwell
584 Scientific Publication, 1-132.
585 V. A, Ponomarchuk., N. L, Dobretsov., E. V, Lazareva., S. M, Zhmodik., N. S,. Karmanov., A. V,. Tolstov., A. N.
586 Pyryaev.,2020. Evidence of Microbial-Induced Mineralization in Rocks of the Tomtor Carbonatite Complex
587 (Arctic Siberia) Doklady Earth Sciences 490,76–80.
588 WANG, CS., DING, XL., 2003. The new researching progress of Tibet plateau uplift. ADVANCE IN EARTH
589 SCIENCES 13(6), 526-532.
590 Wang, HT., Zeng, LS., Gao LE, Hu., ZP, Wang., YF, Zhao., LH., Gao, JH., Xu, Q., 2019. Timing and geochemical
591 characteristics of the Riduo granitic pluton within the Gangdese batholith,southern Tibet. Acta Petrologica
592 Sinica 35 (2), 439-454.
593 Wang, LQ., Zhu, DC., Geng, QR., Liao, ZL., Pan, GT., 2006. The age and significance of the granite porphyry

related to collision in Linzhou basin of Gangdese, Tibet. Chinese Science Bulletin 51(16), 1920-1928 (in Chinese).

Wang, R., Richards, JP., Hou, ZQ., An, F., Creaser, RA., 2015a. Zircon U-Pb age and Sr-Nd-Hf-O isotope geochemistry of the Paleocene-Eocene igneous rocks in western Gangdese: Evidence for the timing of Neo-Tethyan slab breakoff. Lithos 224-225, 179-194

Wang, T., Wang, XX., Guo, L., Zhang, L., Tong, Y., Li, S., Huang, H., Zhang, JJ., 2017 “Granitoid and tectonics”. ActaPetrologica Sinica.33(5), 1459-1478. [in Chinese with English abstract].

Wang, XL., 2017.Some new research progresses and main scientific problems of granitic rocks. Acta Petrologica Sinica33(5), 1445-1458.

Wen, DR., Liu, DY., Chung, SL., Chu, MF., Ji, JQ., Zhang, Q., Song,B., Lee, TY.,YehMW and Lo CH. 2008. Zircon SHRIMP U-Pb ages of the Gangdese batholith and implications for Neotethyan subduction in southern Tibet. Chemical Geology 252(3-4), 191-201.

White, L., Lister, G., 2012. The collision of India With Asia. Journal of Geodynamics 56–57, 7–17.

Wu, FY., Jahn, B.M., Wilde, S.A., et al., Highly Frac-tionated I-Type Granites in NE China (I): Geochronolo-gy and Petrogenesis. Lithos 66(3-4), 241-273.

Wu, FY., Li, XH., Zheng, YF., Gao, S., 2007. Lu-Hf isotopic systematics and their applications in petrology. Acta Petrologica Sinica 23(2),185-220 (in Chinese with English abstract)

Wu YB and Zheng YF. 2004. Genesis of zircon and its constraints oninterpretation of U-Pb age. Chinese Science Bulletin49(15), 1554-1569.

Xie, BJ.,Zhou, S.,Xie, GG,Tian, MZ., Liao, ZL., 2013. Zircon SHRIMP U-Pb data and regional contrasts of geochemical characteristics of Linzizong volcanic rocks from Konglong and Dinrenle region,middle Gangdese Belt. Acta Petrologica Sinica, 29(11): 3803-3814.

Xie, JC., Li, WK., Dong, GC, Mo, XX, Zhao, ZD,Yu, JC., Wang, TC. 2013. Petrology,geochemistry and tectonic significance of the granites from Basu area, Tibet. Acta Petrologica Sinica, 29(11):3779-379

Xu WC. Spatial variation of zircon U-Pb ages and Hf isotopiccompositions of the Gangdese granitoids and its geologic implications.Ph. D. Dissertation. Wuhan: China University of Geosciences,1-96(2010)[in Chinese with English summary].

Yan, JJ., Zhao, ZD., Liu, D., Wang, ZZ., Tang, Y., 2017 Geochemistry and petrogenesis of the Late Jurassic Xuru Tsobatholith in central Lhasa Terrane,Tibet. Acta Petrologica Sinica33(8), 2437-2453.

Yin A and Harrison TM. 2000. Geologic evolution of the Himalayan-Tibetan orogen. Annual Review of Earth and

624 Planetary Sciences28(1), 211-280.
625 Yin, A., Harrison, TM., 2000.Geologic evolution of the Himalayan-Tibetan orogen. Annual Review of Earth and
626 Planetary Sciences28, 211-280.
627 Yin., Harrison, T M., 2000.Geologic evolution of the Himalayan-Tibet. Orogen Annu. Rev. Earth Planet. Sci 28,
628 211- 80.
629 Yu, F., Li, ZG., Zhao, ZD., Xie, GG., Dong, GC., Zhou, S., Zhu, DC., Mo, XX.,·2010. Geochemistry and
630 implication of the Linzizong volcanic succession in Cuomai area, central-western Gangdese, Tibet·Acta
631 Petrologica Sinica 26(7), 2217-2225. (in Chinese with English abstract)
632 Yue, XY., Ma, RZ., He, XC., Zhou, X., Zhao, YF., 2013.Isotopic Geochemical Characteristics and Geological
633 Significance of Dianzhong Volcanic Rocks in the Coqen Area, Tibet, China. XINJIANG GEOLOGY 31(3),
634 256-259.
635 Zhang, H., Ji, WQ., Zhang, SH., Wang, JG., Wu, FY., 2019.Zircon U-Pb age and Hf isotope of intrusive rocks
636 from theYawa area in the west part of southern Lhasa terrane,Tibet. Acta Petrologica Sinica 35(2), 423-438.
637 Zhang, LL., Zhu, DC., Zhao, ZD., Liao, ZL., Wang, LQ., Mo, XX., 2011.Early Cretaceous granitoids in
638 Xainza,Tibet:Evidence of slab break-off. Acta Petrologica Sinica 27(7), 1938-1948. (in Chinese with English
639 abstract)
640 Zhang, XQ., Zhu, DC., Zhao, ZD., Sui, QL.,Wang, Q., Yuan, SH., Hu, ZC., Mo, XX., 2012. Geochemistry, zircon
641 U-Pb geochronology and in-situ Hf isotope of the Maiga batholith in Coqen, Tibet: Constraints on the
642 petrogenesis of the Early Cretaceous granitoids in the central Lhasa Terrane. Acta Petrologica
643 Sinica,28(5),1615-1634. (in Chinesewith English abstract)
644 Zhang, Z M., Dong, X., Xiang, H., Liou, J G., Santosh, M., 2013.Building of the deep Gangdese arc, South Tibet:
645 Paleocene plutonism and granulite-facies metamorphism. Journal of Petrology 54, 2547-2580.
646 ZHANG, Zeming., DONG, Xin., GENG, Guansheng., WANG, Wei., YU, Fei., LIU, Feng., 2010. Precambrian
647 Metamorphism of the Northern Lhasa Terrane,South Tibet and Its Tectonic Implications 84(4), 449-456. (in
648 Chinesewith English abstract)
649 Zhang, ZM.,Ding, L., Zhao, ZD., 2017.Santosh, M., Tectonic evolution and dynamics of the Tibetan Plateau.
650 Gondwana Research 41, 1-8.
651 Zheng, K., Wu, CL., Wei, CJ., Gao, YH., Guo, WF., Chen, HJ., Wu, Di., Gao, D., 2019 . Geochemistry, zircon U-
652 Pb geochronology and Hf isotopic characteristics for syenogranite and diorite from the western segment of
653 North Altyn. ActaPetrologica Sinica35(2), 541-557.

Zhou, S., Mo, XX., Dong, GC., Zhao, ZD., Qiu, RZ., Wang, LL., Guo, TY.,2004. The^{40}Ar/^{39} Ar age framework of Linzizong volcanic in Linzhou basin,Tibet, Chinese Science Bulletin 49(20), 2095-2103 (in Chinese)

Zhu, D C., Mo, X X., Niu, Y L., Zhao, Z D., Wang, L Q., Liu, Y S., Wu, F Y., 2009. Geochemical investigation of Early Cretaceous igneous rocks along an east-west traverse throughout the central Lhasa Terrane, Tibet. Chemical Geology 268, 298-312..

Zhu, D C., Zhao, Z D., Niu, Y L., Mo, X X., Chung, S L., Hou, Z Q., Wang, L Q., Wu, F Y., 2011. The Lhasa terrane: Record of a microcontinent and its histories of drift and growth. Earth and Planetary Science Letters, 301, 241-255.

Zhu, DC., Zhao, ZD., Niu, YL., Dilek, Y., Hou, ZQ., Mo, XX., 2013. The origin and pre-Cenozoic evolution of the Tibetan Plateau. Gondwana Research 23(4),1429-1454..